Mon. Not. R. Astron. Soc. **000**, 000–000 (0000) Printed 12 December 2012 (MN LaTeX style file v2.2)

arXiv:1212.2223v1 [astro-ph.CO] 10 Dec 2012

Lessons from cosmic history: The case for a linear star formation – H_2 relation

Robert Feldmann,[1]⋆
[1] *Department of Astronomy, University of California, Berkeley, CA 94720-3411, USA*

12 December 2012

ABSTRACT

Observations show that star formation in galaxies is closely correlated with the abundance of molecular hydrogen. Modeling this empirical relation from first principles proves challenging, however, and many question regarding its properties remain open. For instance, the exact functional form of the relation is still debated and it is also unknown whether it applies at $z > 4$, where CO observations are sparse. Here, we analyze how the shape of the star formation – gas relation affects the cosmic star formation history and global galaxy properties using an analytic model that follows the average evolution of galaxies in dark matter halos across cosmic time. We show that a linear relation with an H_2 depletion time of ~ 2.5 Gyr, as found in studies of nearby galaxies, results in good agreement with current observations of galaxies at both low and high redshift. These observations include the evolution of the cosmic star formation rate density, the $z \sim 4 - 9$ UV luminosity function, the evolution of the mass – metallicity relation, the relation between stellar and halo mass, and the gas-to-stellar mass ratios of galaxies. In contrast, the short depletion times that result from adopting a highly super-linear star formation – gas relation lead to large star formation rates, substantial metal enrichment ($\sim 0.1\ Z_\odot$), and low gas-to-stellar mass ratios already at $z \gtrsim 10$, in disagreement with observations. These results can be understood in terms of an equilibrium picture of galaxy evolution in which gas inflows, outflows, and star formation drive the metallicities and gas fractions toward equilibrium values that are determined by the ratio of the gas accretion time to the gas depletion time. In this picture, the cosmic modulation of the accretion rate is the primary process that drives the evolution of stellar masses, gas masses, and metallicities of galaxies from high redshift until today.

Key words: galaxies: evolution – galaxies: ISM – galaxies: high-redshift – galaxies: star formation

1 INTRODUCTION

The relation between the star formation rate (SFR) per unit area, $\Sigma_{\rm SFR}$, and the gas surface density (of either molecular or neutral gas) has been a focal point of many galaxy evolution studies (Schmidt 1959, 1963; Kennicutt 1989, 1998; Wong & Blitz 2002; Heyer et al. 2004; Gao & Solomon 2004; Krumholz & McKee 2005; Krumholz & Thompson 2007; Bigiel et al. 2008; Robertson & Kravtsov 2008; Gnedin et al. 2009; Krumholz et al. 2009b; Daddi et al. 2010b; Gnedin & Kravtsov 2010; Ostriker et al. 2010; Schruba et al. 2010; Genzel et al. 2010; Gnedin & Kravtsov 2011; Narayanan et al. 2011; Bigiel et al. 2011; Rahman et al. 2011; Feldmann et al. 2011; Rahman et al. 2012; Lada et al. 2012; Feldmann et al. 2012). This relation holds over several orders of magnitude in $\Sigma_{\rm SFR}$ with a relatively small scatter if measured on $\sim$ kpc sized patches of galaxies or for whole galaxies. Yet, despite these efforts, we still do not quite understand how this correlation comes about and, embarrassingly, what the precise functional form of this relation is.

The reason for the latter is that neither SFRs nor molecular hydrogen (H_2) masses are directly accessible in extragalactic observations. SFRs are inferred from a combination of ultraviolet (UV) and infrared (IR) observations, in order to capture the energy output of both obscured and unobscured star formation. Cold molecular gas is measured indirectly from emission lines of tracer molecules, such as car-

---

⋆ Hubble fellow, feldmann@berkeley.edu

© 0000 RAS

bon monoxide (CO). While observational studies of nearby galaxies and galaxies out to $z \sim 3$ seem to show that the relation between $\Sigma_{\rm SFR}$ and $\Sigma_{\rm H_2}$ is close to linear (Bigiel et al. 2008; Daddi et al. 2010a,b; Genzel et al. 2010), there is no clear theoretical understanding why this is and, furthermore, there are potential concerns that systematics in the observables bias these results. For instance, it has been suggested that the star formation – gas relation is super-linear with a power-law exponent of ~ 1.4 on kpc scales, but that IR emission unrelated to recent star formation reduces the inferred slope, see Liu et al. (2011), but cf. Rahman et al. (2011). Alternatively, systematic variation of the CO/H$_2$ conversion factor with CO intensity, SFRs, or gas surface density could potentially disguise a highly super-linear relation and make it appear linear (Narayanan et al. 2011, 2012b), cf. Feldmann et al. (2012). Finally, the fitting itself has been targeted as a potential source of bias. A Bayesian re-analysis of the data presented by Bigiel et al. (2008) results in tentative evidence that the star formation – gas relation is mildly *sub*-linear and shows substantial variations from one galaxy to the next (Shetty et al. 2012).

Theoretical explanations of the star formation – gas connection predict a variety of non-linear relationships, see e.g., Krumholz & McKee (2005); Krumholz et al. (2009b); Ostriker et al. (2010); Ostriker & Shetty (2011); Krumholz et al. (2012). For instance, Krumholz et al. (2009b) estimate that the power-law exponent is mildly non-linear (~ 1.33) at high gas surface densities ($\gtrsim 100$ $M_\odot$ pc^{-2}), while Ostriker & Shetty (2011) predict a much steeper, quadratic relation at such gas surface densities. This gas surface density regime is clearly highly relevant because it corresponds to typical gas surface densities of star forming galaxies at $z \gtrsim 1$ and higher (e.g., Genzel et al. 2010, see also Section 3.2). A significantly super-linear star formation – gas relation has also been suggested by recent work based on (non-cosmological) galaxy evolution simulations that include a $\sim$ pc-scale modeling of various stellar feedback channels (Hopkins et al. 2011, 2012).

In this paper we take a very different approach to put constrains on the functional form of the star formation – gas relation. We study how global galaxy properties vary depending on the chosen star formation – gas relation and compare our model predictions with observations. In particular, we show that the evolution of the cosmic SFR density (SFRD; Lilly et al. 1996; Madau et al. 1996; Steidel et al. 1999) at $z \sim 4 - 10$ (Bouwens et al. 2007, 2012a; Behroozi et al. 2012b) is highly sensitive to the adopted form of the star formation – gas relation, and, hence, that it can be used to test its functional form.

The paper is organized as follows. In Section 2 we describe the analytic model which underlies our predictions and present the star formation – gas relations that enter our analysis. In Section 3.1 we demonstrate that the model reproduces the observed stellar mass – metallicity relation, the stellar mass – halo mass relation, and the gas-to-stellar mass ratios of galaxies reasonably well *if* a linear star formation – gas relation is chosen. We also show that predictions based on a quadratic star formation – gas relation are in conflict with observations. Next, in Section 3.2, we present how the cosmic star formation history is affected by the functional form of the star formation – gas relation. We discuss the origin of this result in Section 3.3. In Section 3.4 we put our findings in a broader context, showing that galaxy evolution can be thought of as an evolution along a line of fixed points (equilibria) driven by the cosmic modulation of the gas accretion rate. Potential caveats of our study are presented in 3.5. We summarize our findings in Section 4 and close the paper with a comparison to previous work.

2 THE MODEL

The analytic model that is used in the remainder of the paper follows closely the approach presented by Bouché et al. (2010) and Krumholz & Dekel (2012). At its most basic level the model tracks the average evolution[1] of the dark matter, gas, and stellar content of halos using theoretically or observationally motivated accretion and transformation rates for the different mass components. For the convenience of the reader we begin by summarizing the main equations that enter the model and refer the reader to Krumholz & Dekel (2012) for more details. We then discuss the various star formation models that we explore in this work and conclude the section with a short descriptions of the actual set-up of the model. In the following, we adopt cosmological parameters consistent with WMAP 7-year data (Komatsu et al. 2011): $\Omega_{\rm m} = 0.27$, $\Omega_{\rm b} = 0.046$, $\Omega_\Lambda = 0.73$, $h = 0.7$, and $\sigma_8 = 0.81$.

2.1 Basic equations

Accretion rates: The total (baryon plus dark matter) accretion rate at time t onto a halo of a given mass $M_{\rm halo}$ is (Neistein et al. 2006; Neistein & Dekel 2008; Krumholz & Dekel 2012)

$$\dot{M}_{\rm halo} = 1.06 \times 10^{12} M_\odot \left(\frac{M_{\rm halo}}{10^{12} M_\odot}\right)^{1.14} \frac{\dot{D}(t)}{D(t)^2}. \quad (1)$$

$D(t)$ is the linear growth factor normalized to unity at the present epoch. The (average) evolution of the mass of a halo can be computed from its initial mass and the time- and mass-dependent accretion rate (1). The corresponding accretion rates of the gas and stellar components are

$$\dot{M}_{\rm g,in} = \epsilon_{\rm in} f_{\rm g,in} f_{\rm b}\, \dot{M}_{\rm halo}, \quad (2)$$

$$\dot{M}_{*,\rm in} = (1 - f_{\rm g,in}) f_{\rm b}\, \dot{M}_{\rm halo}. \quad (3)$$

Here, $\epsilon_{\rm in}$ specifies which fraction of the accreted gas reaches the galaxy at the center of the halo, $f_{\rm b} = \Omega_{\rm b}/\Omega_{\rm m}$ is the cosmic baryon fraction, and $f_{\rm g,in}$ is the gas fraction (in units of $f_{\rm b}$) of the accreted matter. We assume that accretion of gas onto the disk is completely quenched ($\epsilon_{\rm in} = 0$) when the halo mass is above the virial shock mass $M_{\rm shock}(z)/10^{12} M_\odot = \max(2, 10^{12} M_\odot/(3 M_{*,\rm PS}))$ (Dekel et al. 2009; Krumholz & Dekel 2012). Here, $M_{*,\rm PS}(z)$ is the Press-Schechter mass at the given redshift, see

---

[1] Since the model does not use merger trees, it only follows the mean evolution of halos. For the quantities studied in this paper (the cosmic star formation history and the gas fraction of galaxies), such an average description is adequate.

Mo & White (2002). Accretion is also quenched when the halo mass is so low that photo-ionization limits the baryon fraction in the halos to 50% of f_b or less (Hoeft et al. 2006; Okamoto et al. 2008). Specifically we assume $\epsilon_\mathrm{in} = 0$ if the halo mass is below the mass $M_\mathrm{c}(z)$ given in Fig. 3 of Okamoto et al. (2008). We adopt $M_\mathrm{c} = 0$ for $z \geqslant 9$. We assume that accretion is not quenched ($\epsilon_\mathrm{in} = 1$) if the halo mass lies between M_c and M_shock. We compute $f_\mathrm{g,in}$ as described by Krumholz & Dekel (2012). In brief, we first compute which fraction of the accretion rate is due to accreted halos of a given mass. The model provides us directly with the gas fraction of a halo of a given mass and we then calculate $f_\mathrm{g,in}$ as the accretion-weighted mean gas fraction (in units of f_b) of all accreted halos plus an additional non-halo contribution of 20%.

Evolution of the gas and stellar mass: Besides accretion, the baryonic components are subject to additional physical processes, such as star formation, stellar mass loss, and galactic outflows which we consider next. Specifically, we assume that the gas and stellar masses change according to

$$\dot{M}_\mathrm{g} = \dot{M}_\mathrm{g,in} - (1 - R + \epsilon_\mathrm{out})\dot{M}_\mathrm{*,form}, \tag{4}$$

$$\dot{M}_* = \dot{M}_\mathrm{*,in} + (1 - R)\dot{M}_\mathrm{*,form}. \tag{5}$$

$\dot{M}_\mathrm{*,form}$ is the SFR of the galaxy (see below). R is the fraction of the stellar mass of a single stellar population that is recycled to the ISM via, e.g., stellar winds. For the IMF assumed in this work (Chabrier 2005), $R = 0.46$ is appropriate. The model makes the simplifying assumption of instant recycling which is, however, adequate for our purposes (Krumholz & Dekel 2012). The parameter ϵ_out is included to model large scale galactic outflows. We follow Krumholz & Dekel (2012) and assume $\epsilon_\mathrm{out} = 1$, i.e., a gas outflow rate equal to the SFR, based on the estimates by (Erb 2008). We discuss the impact of varying this and other model parameters in Section 3.5.

The gas disk: For the modeling of the star formation (see below) we need to know how the gas is distributed in the galaxy. We make the ansatz that the gas forms an exponential disk, see e.g., Bigiel & Blitz (2012),

$$\Sigma_\mathrm{g}(r) = \Sigma_\mathrm{g}(0)\exp^{-r/R_d}. \tag{6}$$

We assume that the scale radius R_d is set by the initial, pre-collapse angular momentum of the gas (Mo et al. 1998). Specifically,

$$R_\mathrm{d} = 0.5\lambda R_\mathrm{vir}, \tag{7}$$

where $R_\mathrm{vir}(M_\mathrm{halo}, z)$ and $\lambda = 0.07$ (Krumholz & Dekel 2012) are the virial radius and (median) spin parameter of the halo, respectively. The prefactor takes into account that the half-mass radius of an exponential disk is $\sim 1.7R_\mathrm{d}$. The predictions of equation (7) are in reasonable agreement with observations. Bigiel & Blitz (2012) find a mean scale radius of 6.1 ± 0.7 kpc (with significant galaxy-to-galaxy variations) for a sample of roughly MW-like galaxies in the local Universe, while equation (7) predicts $R_\mathrm{d} \sim 9$ kpc for a 10^{12} $M_\odot$ halo at $z = 0$. Reducing λ to a more traditional value $\lambda \sim 0.04 - 0.05$ (Barnes & Efstathiou 1987; Bullock et al. 2001; Dutton et al. 2011), would lead to even better agreement, see also Section 3.5.

Molecular hydrogen: The abundance of molecular gas plays an important role in many of the star formation models that we consider in the paper (see below). We compute the H_2 surface density $\Sigma_{\mathrm{H}_2} = f_{\mathrm{H}_2}\Sigma_\mathrm{g}$ following Krumholz et al. (2008, 2009a):

$$f_{\mathrm{H}_2}(\Sigma_\mathrm{g}, Z) = \begin{cases} 1 - \frac{0.75s}{1+0.25s}, & \text{if } s < 2 \\ 0, & \text{otherwise} \end{cases} \tag{8}$$

$$s = \frac{\ln(1 + 0.6\chi + 0.01\chi^2)}{0.6\tau_c} \tag{9}$$

$$\chi = \frac{3.1}{4.1}\left(1 + 3.1(Z/Z_\odot)^{0.365}\right) \tag{10}$$

$$\tau_c = 320\,c\,\frac{\Sigma_\mathrm{g}}{\mathrm{gcm}^{-2}}Z/Z_\odot,\ c = 5. \tag{11}$$

Here, $Z = M_\mathrm{Z}/M_\mathrm{g}$ is the average metallicity of the gas and we effectively assume that there are no strong metallicity gradients. We note that gas disks in nearby galaxies often show a moderate radial metallicity gradient of the order of $\sim 0.05 - 0.1$ dex per kpc (Zaritsky et al. 1994), corresponding to a factor $\sim 1.5 - 4$ decrease in oxygen abundance from the center to the optical edge of the disk (Moustakas et al. 2010). We discuss how metallicity gradients affect our results in Section 3.5.

Metallicity evolution: The dependence of the H_2 abundance on the metallicity[2] of the ISM requires that we keep track of the build-up of metals in each galaxy. In the instantaneous recycling approximation and ignoring inflows and outflows the total metal production rate is proportional to both the yield y of the stellar population and the star formation rate, i.e., $\dot{M}_\mathrm{Z,tot} = y(1 - R)\dot{M}_\mathrm{*,form}$. Metals that are locked in stellar remnants do not contribute to the metallicity of the ISM, which therefore evolves according to $\dot{M}_\mathrm{Z} = y(1 - R)\dot{M}_\mathrm{*,form} - Z(1 - R)\dot{M}_\mathrm{*,form}$. As suggested by Krumholz & Dekel (2012) we add three processes to the basic picture. First, a fraction $\zeta(M_\mathrm{halo}) = 0.9\,\exp(-M_\mathrm{halo}/3 \times 10^{11} M_\odot)$ of the newly produced metals (predominantly in a hot, shocked phase) is removed from small halos by supernovae driven outflows. Second, cold and warm gas of the ISM and the associated metals are lost by galactic winds at a rate $\epsilon_\mathrm{out}(M_\mathrm{Z}/M_\mathrm{g})\dot{M}_\mathrm{*,form}$. Third, inflows from the IGM add metals at the rate $Z_\mathrm{IGM}\dot{M}_\mathrm{g,in}$. Hence, the total metal mass of a galaxy changes according to

$$\dot{M}_\mathrm{Z} = \left[y(1 - R)(1 - \zeta) - (1 - R + \epsilon_\mathrm{out})M_\mathrm{Z}/M_\mathrm{g}\right]\dot{M}_\mathrm{*,form} + Z_\mathrm{IGM}\dot{M}_\mathrm{g,in}. \tag{12}$$

A single pair instability supernova can enrich halos at high redshifts to metallicities $\sim 2 \times 10^{-5}$ (Wise et al. 2012). We therefore adopt the value $Z_\mathrm{IGM} = 2\times10^{-5}$ as the metallicity of both the initial gas and the gas accreted onto halos.

Differences to Krumholz & Dekel (2012): Our implementation of the model follows closely the approach presented by Krumholz & Dekel (2012). The only noteworthy differences are the following.

---

[2] More precisely, it is the dust-to-gas ratio that regulates the abundance of H_2. We assume that the dust-to-gas ratio scales proportional with metallicity as observed for galaxies enriched to $Z \gtrsim 0.1\,Z_\odot$ Leroy et al. (2011).

- We added a mass threshold below which gas accretion is quenched due to photo-ionization.
- The metallicity evolution of the ISM (Equation 12) accounts for the locking-up of metals in stellar remnants. Mathematically this amounts to replacing $\epsilon_{\rm out}$ in Equation 23 of Krumholz & Dekel (2012) with $\epsilon_{\rm out} + (1 - R)$ and, hence, is equivalent to a change of the parameter $\epsilon_{\rm out}$. We show in Section 3.5 that varying $\epsilon_{\rm out}$ by a factor of a few does not strongly affect the SFRDs at $z > 2$.
- We use a variety of different star formation – gas relations (see next section).

2.2 Star formation

We calculate the SFR of a galaxy by converting a gas surface density (either the total gas or the H$_2$ surface density) into a SFR surface density with the help of an empirically motivated or theoretically derived star formation – gas relation. The SFR of a galaxy is then simply the integral of the SFR surface density over the area of the gas disk of the galaxy.

A variety of star formation – gas relations have been suggested based on theoretical modeling and/or observations. The relationship often takes the form of a power-law with an exponent between approximately 1 (linear) and 2 (quadratic). In this paper we primarily focus on the two limiting cases out of the many possibilities for the following reasons. First, comparing a linear with a quadratic relation makes the qualitative changes in global galaxy properties more apparent that arise from the functional form of the star formation – gas relation. Second, we find that relations with exponents intermediate between the linear and the quadratic case result in corresponding intermediate predictions. Hence, much can be learned already from a study of the more extreme cases. Finally, both the linear and the quadratic star formation – gas relation are supported by various lines of evidence. It is thus clearly of high interest to test their specific implications for the evolution of galaxy properties.

An approximately linear relation is empirically motivated by observational studies of the $\Sigma_{\rm SFR} - \Sigma_{\rm H_2}$ relation in the local universe (Bigiel et al. 2008, 2011) and out to, at least, $z \sim 2$ (Genzel et al. 2010). The depletion time in nearby galaxies is $\sim 2 - 3$ Gyr (Bigiel et al. 2011), but whether this is also true at high redshift is not so clear, see, e.g., Tacconi et al. (2012). High redshift samples typically include only galaxies with large star formation rates and gas masses, and, hence, in case of a slightly super-linear star formation – gas relation it is difficult to distinguish a change in the depletion time with redshift from a change in depletion time due to the increase in gas surface density. Uncertainties in the CO/H$_2$ conversion factor and the limited spatial resolution of CO observations further complicate an accurate measurement of the depletion time at high redshift. A quadratic relationship (at gas surface densities $\gtrsim 50\ M_\odot\ {\rm pc}^{-2}$) is expected based on analytic and numerical models of feedback-regulated star formation, e.g., Ostriker & Shetty (2011). It has also been argued that a quadratic relationship is supported by current observations once the conversion between CO emission and H$_2$ surface density is properly taken into account (Narayanan et al. 2012b, but cf. Feldmann et al. 2012).

In addition to the mentioned linear and quadratic relationship we also explore how alternative star formation – gas relations would affect the cosmic star formation history. In the following Σ may refer to either the H$_2$ surface density $\Sigma_{\rm H_2} = f_{\rm H_2}(\Sigma_{\rm g}, Z)\Sigma_{\rm g}$ (the default), to the H$_2$ surface density $\Sigma_{{\rm H_2},Z_\odot} = f_{\rm H_2}(\Sigma_{\rm g}, Z_\odot)\Sigma_{\rm g}$ for gas of solar metallicity, or to the total gas surface density, $\Sigma_{\rm g}$, respectively. The full list of star formation – gas relations used in this paper is the following:

- A *linear relation* with a constant depletion time of 2.5 Gyr (Bigiel et al. 2011), i.e.,

$$\Sigma_{\rm SFR} = \frac{\Sigma}{2.5\,{\rm Gyr}}. \tag{13}$$

- A relation that is *quadratic* at gas surface densities $\geqslant 50\ M_\odot\ {\rm pc}^{-2}$ and linear at smaller surface densities (Ostriker & Shetty 2011):

$$\Sigma_{\rm SFR} = \begin{cases} 0.1\,M_\odot\,{\rm yr}^{-1}\,{\rm kpc}^{-2}\left[\frac{\Sigma}{M_\odot\,{\rm pc}^{-2}}\right]^2 & \text{if } \Sigma_{\rm g} \geqslant 50\,M_\odot\,{\rm pc}^{-2} \\ \frac{\Sigma}{2\,{\rm Gyr}} & \text{if } \Sigma_{\rm g} < 50\,M_\odot\,{\rm pc}^{-2}. \end{cases} \tag{14}$$

The $z \gtrsim 3$ predictions of this star formation – gas relation are effectively indistinguishable from the predictions of a relation that extends the quadratic relationship to $\Sigma_{\rm g} < 50\,M_\odot\,{\rm pc}^{-2}$, because surface densities of star forming galaxies at high redshift typically exceed $50\,M_\odot\,{\rm pc}^{-2}$, see Section 3.2.

- A relation with a moderately sub-linear exponent 0.84 as suggested by Shetty et al. (2012) (with $\Sigma = \Sigma_{\rm H_2}$) :

$$\Sigma_{\rm SFR} = \left(\frac{\Sigma}{10\,M_\odot\,{\rm pc}^{-2}}\right)^{0.84}\frac{10\,M_\odot\,{\rm pc}^{-2}}{2.5\,{\rm Gyr}} \tag{15}$$

- A moderately super-linear relation suggested by Krumholz et al. (2009b) (with $\Sigma = \Sigma_{\rm H_2}$):

$$\Sigma_{\rm SFR} = \frac{\Sigma}{2.6{\rm Gyr}}\begin{cases}\left(\frac{\Sigma_{\rm g}}{85{\rm M}_\odot\,{\rm pc}^{-2}}\right)^{-0.33}, & \text{if } \Sigma_{\rm g} < 85\,{\rm M}_\odot\,{\rm pc}^{-2} \\ \left(\frac{\Sigma_{\rm g}}{85{\rm M}_\odot\,{\rm pc}^{-2}}\right)^{0.33}, & \text{if } \Sigma_{\rm g} \geqslant 85\,{\rm M}_\odot\,{\rm pc}^{-2}. \end{cases} \tag{16}$$

- The "universal" star formation relation suggested by Krumholz et al. (2012) (with $\Sigma = \Sigma_{\rm H_2}$):

$$\Sigma_{\rm SFR} = 0.01\frac{\Sigma}{t_{\rm ff}},\ \text{where } t_{\rm ff} = \min(t_{\rm ff,GMC}, t_{\rm ff,T}), \tag{17}$$

and

$$t_{\rm ff,GMC} = \frac{\pi^{1/4}}{\sqrt{8}}\frac{\sigma}{G(\Sigma_{\rm GMC}^3\Sigma_{\rm g})^{1/4}},\ \Sigma_{\rm GMC} = 85M_\odot{\rm pc}^{-2}, \tag{18}$$

$$t_{\rm ff,T} = \frac{\pi}{8}\frac{1}{\Omega} \tag{19}$$

In Equation (18), σ is the gas velocity dispersion on scales comparable to the disk scale height (few 100 pc). We set it to 8 km/s, adequate for disk galaxies in the local universe (Walter et al. 2008). High redshift galaxies may have larger velocity dispersions (Tacconi et al. 2010), but since typically $t_{\rm ff,GMC} > t_{\rm ff,T}$ for these galaxies (Krumholz et al. 2012), the choice of σ does not matter in this case. Equation (19) includes the angular velocity of galactic rotation Ω. We

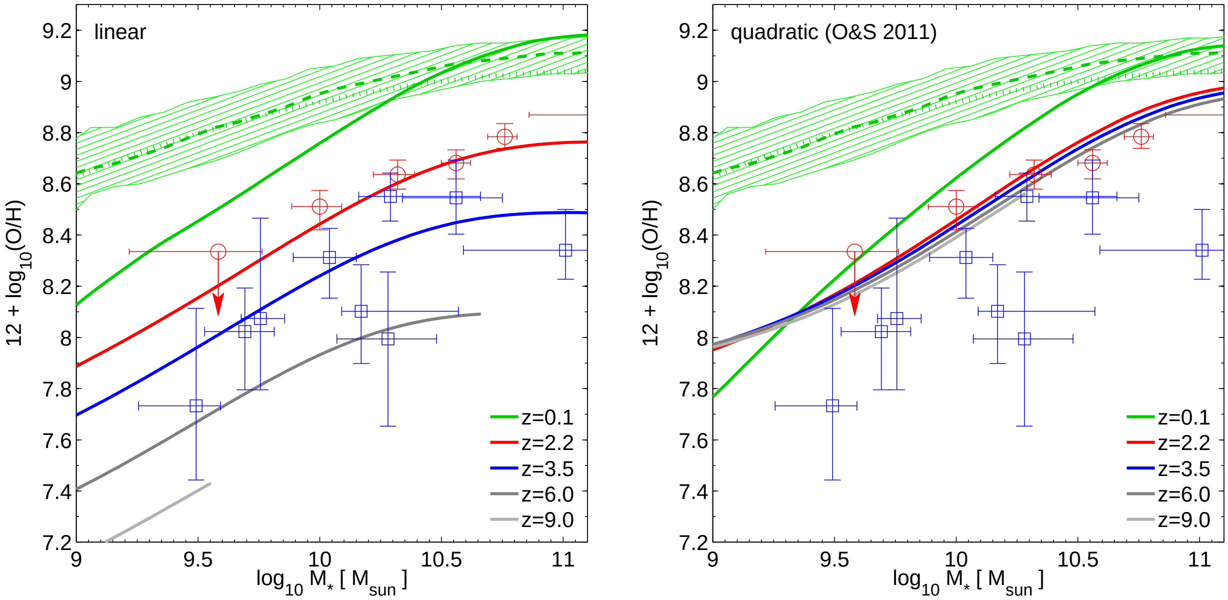

Figure 1. Metallicity vs stellar mass. (Left) Model predictions based on a linear $\Sigma_{\rm SFR} - \Sigma_{\rm H_2}$ relation, Equation (13). (Right) Model predictions based on the quadratic relation given by Equation (14). Solid lines are the model predictions for $z = 0.1$, $z = 2.2$, $z = 3.5$, $z = 6.0$, and $z = 9.0$ (see legend). The dot-dashed line (median) and the shaded region (1-σ scatter) at the top show the observed low redshift ($z \sim 0.1$) mass-metallicity relation from SDSS (Tremonti et al. 2004). The dotted line shows the results of a re-analysis of the Tremonti et al. (2004) study by Kewley & Ellison (2008). Circles and squares are observational estimates for $z \sim 2.2$ (based on stacked spectra; Erb et al. 2006) and for $z \sim 3.5$ (individual galaxies), respectively, by Maiolino et al. (2008), who use the same IMF and metallicity calibrations as Kewley & Ellison (2008). Predictions based on a linear $\Sigma_{\rm SFR} - \Sigma_{\rm H_2}$ relation with a constant ~ 2.5 Gyr depletion time are in good agreement with observations of the mass-metallicity relation at $z \gtrsim 2$.

chose $\Omega = V_{\rm rot}/(1.7\,R_{\rm d})$ as our fiducial value. Here, $1.7\,R_{\rm d}$ is the half-mass radius of the gas disk and $V_{\rm rot}$ is the rotation velocity of the disk at $1.7\,R_{\rm d}$. The latter we equate with $V_{\rm max,h}$, the maximum circular velocity of a dark matter halo with NFW profile (Navarro et al. 1997) that hosts the given galaxy. We determine $V_{\rm max,h}$ for a halo of given mass and at a given redshift using the fits (converted to our definition of halo mass) by Prada et al. (2012) based on high resolution N-body simulations (Klypin et al. 2011). The ansatz $V_{\rm rot} \approx V_{\rm max,h}$ has a firm observational justification, at least for disk galaxies in the local universe (Reyes et al. 2012). In compact star formation galaxies at high redshift, however, it is conceivable that $V_{\rm rot}$ exceeds $V_{\rm max,h}$. If the latter is true, we potentially overestimate $t_{\rm ff,T}$ and, hence, potentially underestimate the SFR at high redshift. As we will show in Section 3.2, this only increases the conflict between this particular star formation – gas relation and observations.

2.3 Running the model

We have implemented the model described in the previous sections as a GNU Octave[3] program. We adopt the fiducial choice of Krumholz & Dekel (2012) (see their Table 1) for the model parameters, and note that most values are justified based on either theoretical grounds (e.g., the recycling fraction R is a consequence of the adopted IMF) or on observations (e.g., $f_{\rm b}$, y). We discuss the robustness of our predictions to changes in the parameter values in Section 3.5.

We assume that each halo initially contains a fraction $f_{\rm b} \sim 0.17$ of its total mass in baryons. The large majority of the baryons is assumed to be in a gaseous component (90%) with an initial metallicity of $Z_{\rm IGM} = 2\times10^{-5}$. The remaining 10% are locked up in a stellar component formed during mergers at high redshift (Rodighiero et al. 2011). We checked that decreasing the initial stellar contribution from 10% to 1% (and increasing the initial gas contributions correspondingly) does not change any of our results in a significant way. We start the model at $z = 30$ and run it forward until $z = 0$ in 300 steps spaced equally in values of the expansion factor $a = 1/(1+z)$. The model follows the concurrent evolution of 300 halos of different mass ranging from 3.2×10^5 $M_\odot$ to 1.3×10^8 $M_\odot$ at $z = 30$ and from 1.4×10^7 $M_\odot$ to 8×10^{15} $M_\odot$ at $z = 0$ in a logarithmic spacing.

3 RESULTS

In this section, we analyze the importance of the functional form of the star formation – gas relation for various galaxy properties and the cosmic star formation history in the context of the model of Section 2.1. We will show that a strongly non-linear star formation – gas relation results in predic-

---

[3] http://www.gnu.org/software/octave

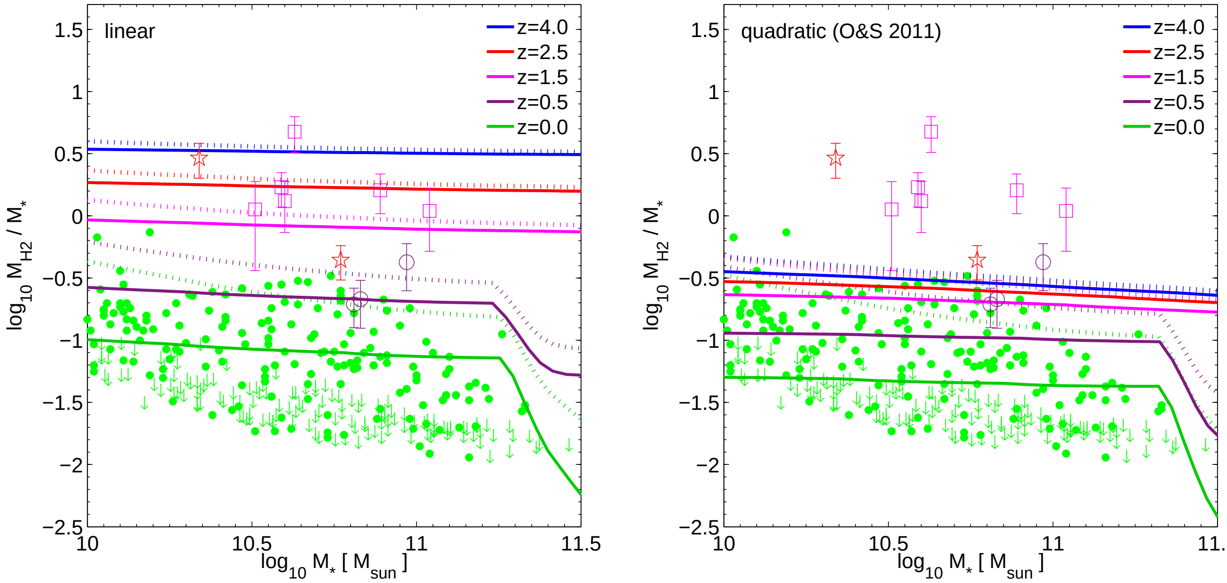

Figure 2. Gas-to-stellar mass ratio in galaxies as function of their stellar mass. (Left) Model predictions based on a linear $\Sigma_{\rm SFR} - \Sigma_{\rm H_2}$ relation, Equation (13). (Right) Model predictions based on the quadratic relation given by Equation (14). The predicted H_2-to-stellar mass ratios are shown by solid lines, while the total gas-to-stellar mass ratio are shown by dotted lines. Different colors correspond to different redshifts as indicated in the legend. The circles (arrows) show $> 3-\sigma$ detections (upper limits) of the H_2 fraction of galaxies in the local universe (Saintonge et al. 2011). Circles ($z \sim 0.5$), squares ($z \sim 1.5$), and stars ($z \sim 2.5$) are measurements of cold gas masses for a sample of galaxies at higher redshift (Magdis et al. 2012a). These latter observations are based on dust infrared emission and are thus not affected by uncertainties related to the CO-H_2 conversion. A linear $\Sigma_{\rm SFR} - \Sigma_{\rm H_2}$ relation predicts a large increase in the gas fractions up to ~ 2 in good agreement with the observed evolution, followed by only a modest change toward higher redshift, cf. Magdis et al. (2012b).

tions that are in conflict with observations, while predictions based on a linear star formation – gas relation match the various observational data better and in most cases remarkably well.

3.1 Metallicities, stellar and gas masses

In Fig. 1 we show the evolution of the stellar mass – metallicity relation as predicted by the model for a linear and a quadratic $\Sigma_{\rm SFR} - \Sigma_{\rm H_2}$ relation, see Equations (13) and (14) with $\Sigma = \Sigma_{\rm H_2}$. We compare these predictions with observations of galaxies at $z \sim 0$ (Tremonti et al. 2004; Kewley & Ellison 2008), at $z \sim 2$ (Erb et al. 2006; Maiolino et al. 2008), and at $z \sim 3.5$ (Maiolino et al. 2008). Predictions based on a linear relation are in excellent agreement with the observed mass – metallicity relation at $z \gtrsim 2$. At low redshifts and low stellar masses the predicted metallicities fall somewhat short of the measured ones, although we could reduce this discrepancy significantly (to less than 0.2 dex) by decreasing the maximum value of ζ (the expelled gas fraction see Section 2) from 0.9 to 0.8, which would also not strongly affect any of our other predictions. A quadratic relation strongly underpredicts the evolution of the mass – metallicity relation at high redshift. The evolution at $z < 2$ is similar to the one for the linear star formation – gas relation, because as those times typical gas surface densities in galaxies falls below $\sim 50\ M_\odot\ {\rm pc}^{-2}$ and the star formation – gas relation is effectively linear , see Equation (14). In fact, if we had used a purely quadratic relation down to low gas surface densities, the mass – metallicity relation would not evolve between $z = 9$ and $z = 0$ - in obvious disagreement with observations.

In Fig. 2 we compare the predicted gas-to-stellar mass ratios with observations spanning the redshift range $z \sim 0-3$. A quadratic star formation – gas relation underpredicts both the total gas- and the molecular gas-to-stellar mass ratios. At $z \sim 0.5$ the model predictions are off by a factor ~ 3. The disagreement becomes even more severe at higher redshift. At $z \sim 2$ the observed gas-to-stellar mass ratios exceed the predicted ones by an order of magnitude. In contrast, we find good agreement between model predictions and observations for both the normalization and the redshift evolution of the gas-to-stellar mass ratio in case of a linear star formation – gas relation. For instance, the predicted fraction $M_{\rm H_2}/(M_{\rm H_2} + M_*)$ is 39% at $z = 1.5$ and 54% at $z = 2.5$, compared with 34% at $z \sim 1.2$ and 44% at $z \sim 2.3$ as found by Tacconi et al. (2010) based on CO observations of a sample of massive star forming galaxies. However, it has been argued that the observed gas masses are potentially overestimated, because of systematic variations of the CO/H_2 conversion factor with CO surface brightness that is unaccounted for Narayanan et al. (2012a). We therefore also compare our predictions with observations that estimate gas masses based on the thermal emission of dust (Magdis et al. 2012a) to circumvent this potential issue. Again, we find

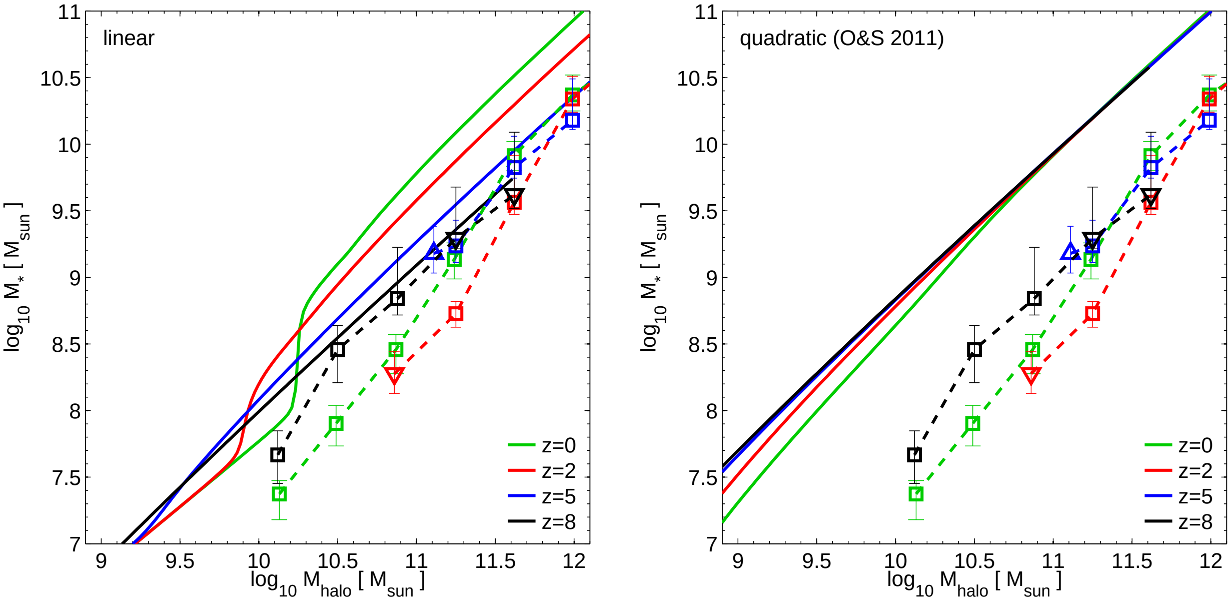

Figure 3. Relation between halo mass and stellar mass of galaxies. (Left) Model predictions based on a linear $\Sigma_{\rm SFR} - \Sigma_{\rm H_2}$ relation, Equation (13). (Right) Model predictions based on the quadratic relation given by Equation (14). Solid lines are the model predictions for $z = 0$, $z = 2$, $z = 5$, and $z = 8$ (see legend). Symbols (color coded according to redshift, see legend) are empirical estimates based on the abundance matching technique (Behroozi et al. 2012a). Because the evolution of the $M_{\rm halo} - M_*$ relation is weak, we combine, for a given redshift z, the abundance matching results from the $z - 1$ (downward pointing triangles), z (squares), and $z + 1$ (upward pointing triangles) redshift bins.

good agreement if the star formation – gas relation is linear, but stark disagreement if the relation is quadratic.

The relation between stellar mass and halo mass of a galaxy is also sensitive to the functional form of the star formation – gas relation, see Fig. 3. Again, a linear star formation – gas relation leads to much better agreement with abundance matching results than a quadratic star formation – gas relation. The agreement is particularly good at high redshifts $z > 4$, where, as we show in the next section, the cosmic star formation history is sensitive to changes in the star formation – gas relation.

3.2 The Cosmic Star Formation History

In Fig. 4 we present the cosmic star formation history as predicted by the model for a linear star formation – H$_2$ relation (Equation 13). Here, the black solid curve shows the contribution of all galaxies sufficiently bright ($\rm M_{UV,AB} < -17.7$) to be accessible to current observations at $z \geqslant 4$. We estimate the luminosity of a galaxy based on its SFR and dust attenuation. For the latter we use Table 6 of Bouwens et al. (2012b) and we extrapolate the multiplicative dust extinction to 1 (no dust extinction) at $z = 10$. For $z < 3$ we assume that the dust extinction remains constant at its value at $z = 3$. The red solid curve shows the contribution of all galaxies down to the photo-ionization limit (Okamoto et al. 2008) to the SFRD. The corresponding dashed curves show what happens if we assume that *all* gas in the disk is molecular, i.e., for $\Sigma = \Sigma_{\rm g}$ in Equation (13). The figure also includes compilations of observational data by Oesch et al. (2012), Bouwens et al. (2012b), and Behroozi et al. (2012b).

An important result of Fig. 4 is that a linear star formation – gas relation predicts a cosmic star formation history that is in good agreement with observational data. Interestingly, given the current observational limits the cosmic star formation history at $z > 2$ changes only by a moderate amount depending on whether star formation is based on molecular hydrogen or not. We can rephrase this result, namely that quenching of star formation in low metallicity and hence H$_2$-poor galaxies at high redshift is not very important for galaxies accessible to observations ($\rm M_{UV,AB} < -17.7$). It does, however, play a crucial role for fainter galaxies. In fact, considering all galaxies the cosmic star formation rate density at $z \sim 10$ is suppressed by 1.5 orders of magnitude if star formation occurs only in molecular gas compared with all the gas in the disk. Obviously, this will have implications for the re-ionization by faint galaxies at such redshifts, see e.g., Kuhlen & Faucher-Giguère (2012), which we plan to address in a follow-up study.

In Fig. 5, we show the predicted UV luminosity function and its evolution with redshift for a linear $\Sigma_{\rm SFR} - \Sigma_{\rm H_2}$ relation and compare it with observations (Bouwens et al. 2012a). The agreement is excellent considering the simplicity of the model and the various observational uncertainties. At $z \sim 8$ the observed luminosity function appears to have a somewhat larger normalization compared with our model predictions, while no such offset is seen at the other redshifts, which could indicate that the $z \sim 8$ observations are affected by cosmic variance. At low luminosities (not shown) the UV luminosity function turns over as a result of the suppression of star formation in low mass halos. Unfortunately, the magnitude at which the turn-over takes place

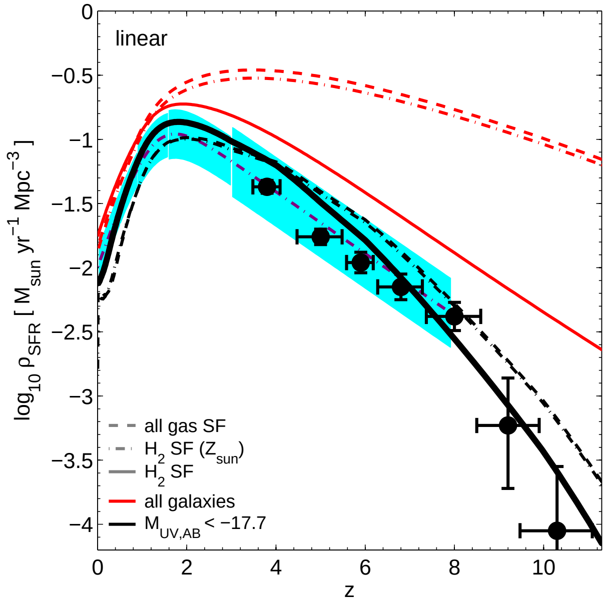

Figure 4. The cosmic star formation history as predicted by the model for a linear $\Sigma_{\rm SFR} - \Sigma_{\rm H_2}$ relation (Equation 13 with $\Sigma = \Sigma_{\rm H_2}$; solid and dot-dashed lines) and a linear $\Sigma_{\rm SFR} - \Sigma_{\rm g}$ relation (Equation 13 with $\Sigma = \Sigma_{\rm g}$; dashed lines), respectively, with a depletion time of 2.5 Gyr (Bigiel et al. 2011). The $\rm H_2$ abundance is computed either based on the current gas metallicity (solid lines) or by assuming that the gas has solar metallicity (dot-dashed lines). Black lines (lower three curves) show the contribution of galaxies bright enough to be accessible to current observations, while red lines (upper three curves) include all galaxies down to the photo-ionization limit (Okamoto et al. 2008). The contribution of galaxies below the current detection limit depends sensitively on whether star formation correlates preferentially with $\rm H_2$ or with the total gas mass in galaxies. Points with error bars are observational constraints from Bouwens et al. (2012b) and should be compared with the black lines. The dot-dashed line and the shaded region in the background show the mean and the typical error of the cosmic star formation history, respectively, as estimated by Behroozi et al. (2012b) using abundance matching and a compilation of observational data from the literature. Predictions based on a linear $\Sigma_{\rm SFR} - \Sigma_{\rm H_2}$ relation with a $\sim$ 2.5 Gyr $\rm H_2$ depletion time are in good agreement with the observed cosmic star formation history.

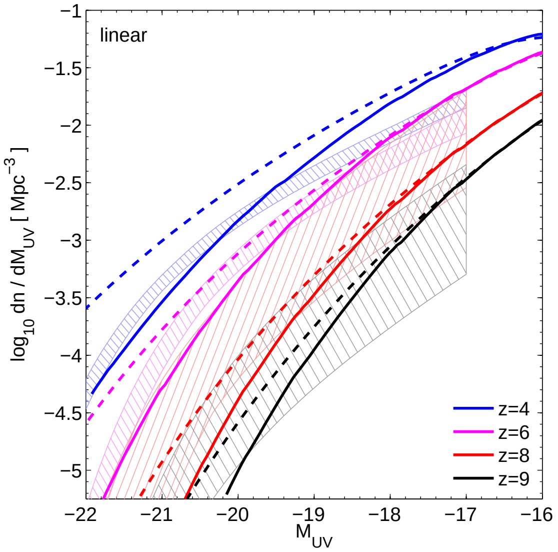

Figure 5. The UV luminosity function as predicted by the model for a linear $\Sigma_{\rm SFR} - \Sigma_{\rm H_2}$ relation with a 2.5 Gyr $\rm H_2$ depletion time. SFRs are converted into UV magnitudes according to $M_{\rm UV} = -2.5 \log_{10}({\rm SFR}/f_{\rm dust}\,[M_\odot\,{\rm yr}^{-1}]) - 18.16$. A 0.1-125 $M_\odot$ Salpeter initial mass function (IMF) and a constant SFR over the last $\gtrsim$ 100 Myr is assumed for the conversion. Solid lines correspond to UV magnitudes that include extinction by dust ($f_{\rm dust} > 1$), while dashed lines show the extinction free predictions ($f_{\rm dust} = 1$). We use the multiplicative dust attenuation factor $f_{\rm dust}(z)$ as given in Fig. 14 of Bouwens et al. (2012b) for $z = 4$ and $z = 6$ (the latter is assumed to hold for $z \sim 6 - 9$), and extend it to faint magnitudes such that $f_{\rm dust} \rightarrow 1$. The hatched regions are measurements of the UV luminosity functions by Bouwens et al. (2012b). We use the Schechter function fits provided in their Table 3 and vary the fit parameters within their quoted error bars to create the hatched regions. The agreement between model predictions and observations is reasonable given the simplicity of the model, the uncertainties in the dust extinction corrections and/or changes in normalization due to cosmic variance.

depends sensitively on model parameters, e.g., on the disk sizes (parametrized by the spin parameter λ), and is therefore not a robust prediction of the model. For instance, at $z \sim 4$ the UV luminosity function is predicted to break at $M_{\rm UV} \sim -15.5$ if we use a linear $\Sigma_{\rm SFR} - \Sigma_{\rm H_2}$ relation with our default choice of model parameters. If, however, we decrease λ from 0.07 to 0.05 the bright end of the luminosity function remains unaffected, while the turn-over shifts to $M_{\rm UV} \sim -12.5$.

In Fig. 6 we show plots analogous to Fig. 4 for four non-linear star formation – gas relation: a moderately sub-linear relation (Equation 15), the moderately super-linear relation postulated by Krumholz et al. (2009b) (Equation 16), the “universal relation” proposed by Krumholz et al. (2012) (Equation 17), and a quadratic relation (Equation 14). The figure clearly demonstrates that a super-linear star formation – gas relation results in SFRDs higher than observed at $z \sim 4 - 10$. The discrepancy is particularly large for strongly non-linear star formation–gas relations, such as the those given by Equations (14) and (17). These relations result in SFRDs that are inconsistent with observations, e.g., at $z = 8$ ($z = 10$) they are one (two) orders of magnitude above observations. Moderately non-linear relations such as those given by Equation (16) and Equation 17) are in tension with observations, but are probably not excluded given the uncertainties of the model.

Similar to Fig. 4, the *observable* SFRD shows no large changes depending on whether star formation takes place only in molecular gas or not. A sub-linear star formation – gas relation leads to the biggest difference ($\sim$ 0.5 dex), while there is almost no change if the relation is strongly super-linear. Furthermore, for a strongly super-linear (e.g., quadratic) star formation – gas relation there is little difference in the star formation history even if galaxies below the observational limits are included. Hence, in this case, quenching of star formation in low metallicity and, thus,

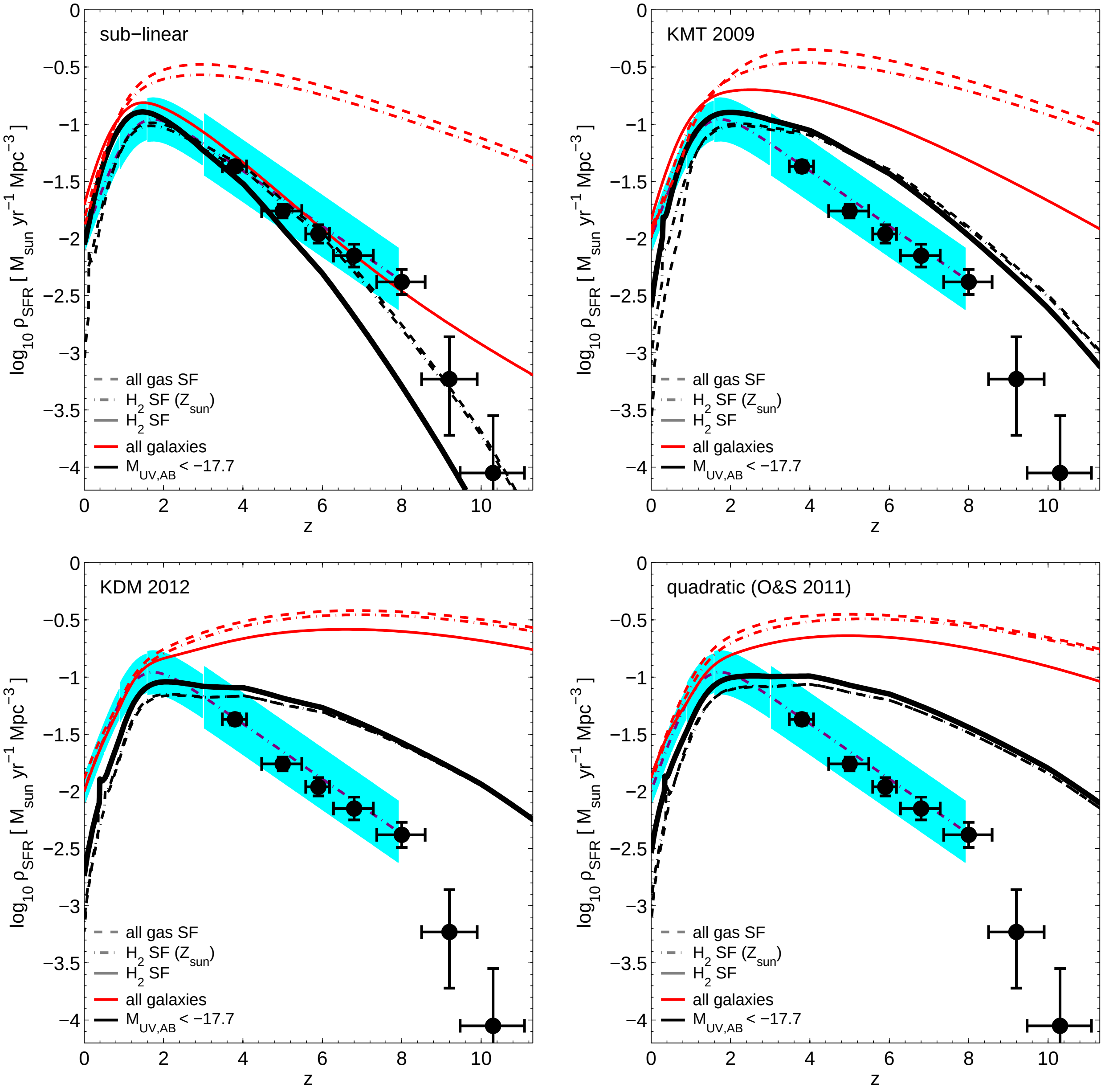

Figure 6. Same as Fig. 4, but for non-linear $\Sigma_{\rm SFR} - \Sigma_{\rm g}$ and $\Sigma_{\rm SFR} - \Sigma_{\rm H_2}$ relations. (Top left) Predictions for a moderately sub-linear relation, see Equation (15). (Top right) Predictions for the moderately super-linear relation suggested by Krumholz et al. (2009b), see Equation(16). (Bottom left) Predictions for the "universal" star formation – gas relation suggested by Krumholz et al. (2012), see Equation (17). (Bottom right) Predictions for a quadratic relation (Ostriker & Shetty 2011), see Equation (14). The observable cosmic star formation history (black lines) is highly sensitive to the functional form of the star formation – gas relation.

H$_2$-poor galaxies is not affecting the cosmic star formation history.

Before we address this last point, let us understand why the SFRD depends sensitively on the functional form of the star formation – gas relation if star formation is based on the abundance of H$_2$. We show in Fig. 7 the evolution of the typical gas surface density (here $\Sigma_{\rm g}(r_{1/2})$, the surface density at the gas half mass radius) of galaxies residing in halos of different mass. At $z \sim 20 - 30$ this surface density is typically in the range $300 - 1000$ $M_\odot$ pc^{-2}. As the universe expands, gas surface densities in galaxies decrease and reach values in agreement with observations of nearby galaxies (~ 10 $M_\odot$ pc^{-2} for galaxies in halos with masses $\sim 10^{11} - 10^{12}$ $M_\odot$, e.g., Wong & Blitz 2002). Galaxies in halos above the virial shock quenching mass ($\gtrsim 2 \times 10^{12}$ $M_\odot$) experience a fast decline in their gas surface density at low redshift caused by the shut-down of gas accretion.

We also include in the figure the evolution of the critical surface density $\Sigma_{\rm g}(f_{\rm H_2} = 0.5)$ required to turn half the gas molecular. We note that there is a one-to-one correspon-

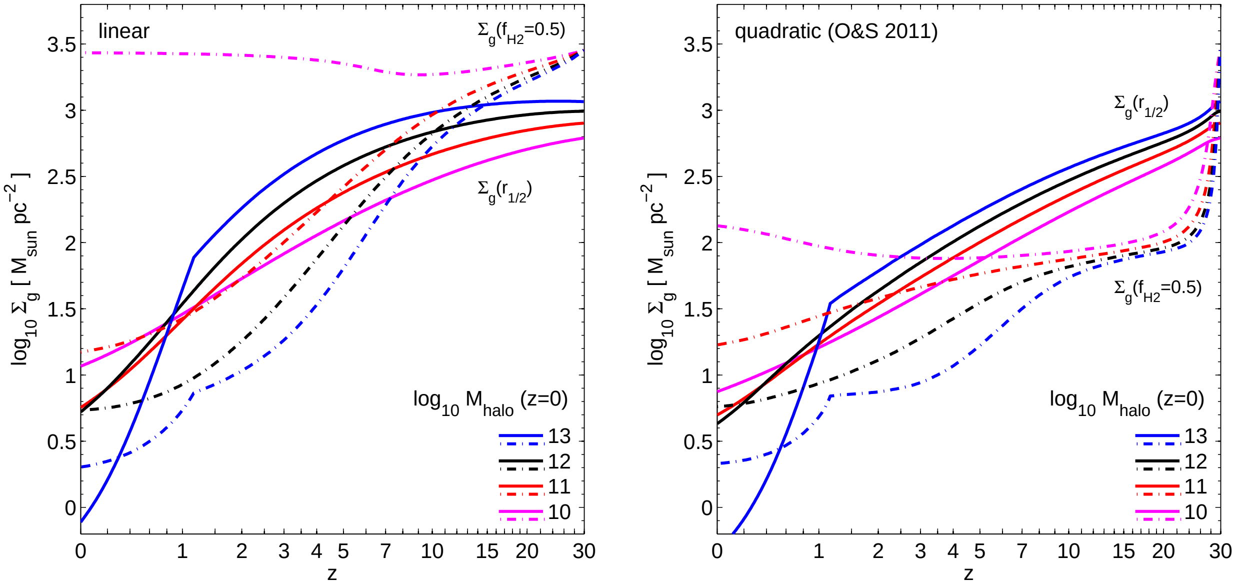

Figure 7. Evolution of the gas surface density at the disk half mass radius ($\Sigma_g(r_{1/2})$, solid lines) and evolution of the surface density at which the molecular fraction is 50% ($\Sigma_g(f_{H_2} = 0.5)$, dot-dashed lines) for halos of different masses (see legend). (Left) for a linear star formation – gas relation (Equation 13 with $\Sigma = \Sigma_{H_2}$). (Right) for a quadratic star formation – gas relation (Equation 14 with $\Sigma = \Sigma_{H_2}$). The expansion of the universe, the consumption of gas, and the quenching of gas accretion result in a reduction of $\Sigma_g(r_{1/2})$ with time. Star formation increases the metallicity and thus decreases $\Sigma_g(f_{H_2} = 0.5)$ (Equation 8). A quadratic star formation – gas relation leads to early enrichment (to $\sim 0.1\ Z_\odot$ already at $z \gtrsim 10$). Enrichment proceeds much more slowly in case of a linear $\Sigma_{\rm SFR} - \Sigma_{H_2}$ relation.

dence between this critical surface density and the metallicity of the gas, see Equation (8). Initially the critical surface density is large $\sim 3000\ M_\odot$ pc^{-2} (corresponding to $Z_{\rm IGM} = 2 \times 10^{-5}$), but it decreases with time as metal enrichment by star formation boosts the molecular content of the gas. Clearly, the choice of the star formation – gas relation has a large impact on the evolution of this critical surface density or, equivalently, the metallicity. If the star formation – gas relation is linear, halos with $z = 0$ masses below $\sim 3 \times 10^{10}\ M_\odot$ are unable to significantly increase the metallicity of the gas. In contrast, efficient enrichment can take place in such halos at early times ($z > 10$) if the relation is non-linear.

In Fig. 8 we compare the ratio between the typical gas surface density, $\Sigma_g(r_{1/2})$, and the critical surface density, $\Sigma_g(f_{H_2} = 0.5)$. H_2-based star formation can only take place throughout the disk if this ratio is $\gtrsim 1$. If the star formation – gas relation is linear, gas in galaxies with $z = 0$ halo masses below $\sim 3 \times 10^{10}\ M_\odot$, remains effectively unenriched and thus atomic. Hence, star formation is almost completely quenched in halos of such mass. However, galaxies in more massive halos are able to turn a substantial fraction of their gas reservoir into H_2. In fact, the condition $\Sigma_g(r_{1/2}) \sim \Sigma_g(f_{H_2} = 0.5)$ is satisfied increasingly earlier for halos of higher mass, e.g., at $z \sim 10$ ($z \sim 4.5$) for halos with $z = 0$ masses of $10^{12}\ M_\odot$ ($10^{11}\ M_\odot$). If the star formation – H_2 relation is quadratic, galaxies generally reach metallicities of $Z \sim 2 \times 10^{-3}$ (a tenth solar) quickly after a single Pop III star initially enriches the gas to $Z \sim 2 \times 10^{-5}$. Hence, most galaxies, even those in low mass halos, have fully molecular gas disks and are able to form stars efficiently at early times. This also explains why the metallicity-dependent quenching of star formation has little impact on the cosmic star formation history in this case. Early enrichment ($\sim 0.1\ Z_\odot$) and high gas surface densities ($\gtrsim 100\ M_\odot$ pc^{-2}) ensure that most of the gas in galaxies is molecular at $z > 4$, even in low mass halos, and thus it does not matter whether Σ_{H_2} or Σ_g is the gas surface density relevant for star formation.

Returning to the discussion of the linear star formation – gas relation, it is important to point out that the lack of early enrichment is *not* the reason that $\lesssim 3 \times 10^{10}\ M_\odot$ halos are inefficient star formers at observationally accessible redshifts $z \lesssim 10$. To show this we re-run the model for the linear relation with a 100 times higher initial gas metallicity of the halos, i.e., with $Z = 2 \times 10^{-3}$ instead of 2×10^{-5}, see Fig. 8. Clearly, the ratio between typical and critical gas surface density is not affected in a significant way at $z \lesssim 10$. In particular, galaxies with $z = 0$ halo masses below $3 \times 10^{10}\ M_\odot$ still do not contribute to star formation at these redshifts.

We conclude that while star formation follows the metal enrichment of the gas, the evolution of the latter is primarily driven by the functional form of the star formation – gas relation. A non-linear relation leads to fast enrichment and, hence, to galaxy disks that are fully molecular and have large star formation rates even in low mass halos at high redshifts. In contrast, a linear relation delays the enrichment of the gas and therefore limits star formation to sufficiently massive halos.

This leaves us with one open question, namely how can the star formation – gas relation have such a strong impact

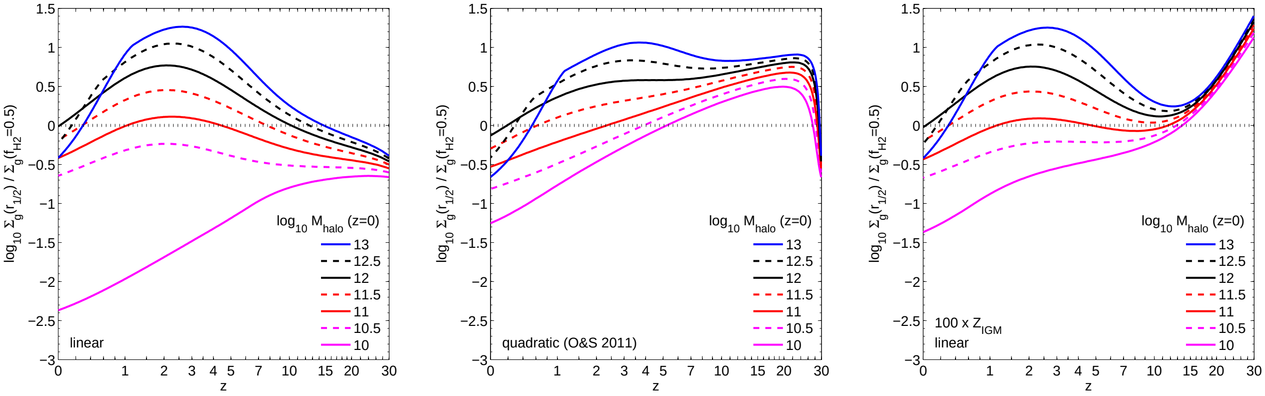

Figure 8. Evolution of the ratio between the typical gas surface density in a disk, $\Sigma_g(r_{1/2})$, and the surface density at which the molecular fraction is 50%, $\Sigma_g(f_{H_2} = 0.5)$, see Fig. 7. A ratio significantly below (above) unity means that most of the gas in the disk of a galaxy is atomic (molecular). (Left) for a linear star formation – gas relation (Equation 13 with $\Sigma = \Sigma_{H_2}$). Gas surface densities become sufficiently large to form molecules and stars only in massive halos at sufficiently late times. (Middle) for a quadratic star formation – gas relation (Equation 14 with $\Sigma = \Sigma_{H_2}$). A strongly super-linear star formation – gas relation allows the formation of fully molecular gas disks at earlier times and in halos of lower masses and, hence, boosts the star formation rate at the relevant, and observationally accessible, redshift range $z \sim 4 - 10$. (Right) same as left panel, but with the metallicity of the gas in the galaxy disks initially set to $Z = 0.1\ Z_\odot$. The $z \lesssim 10$ evolution is hardly affected by this dramatic change, demonstrating that the lack of early enrichment is not the reason that a linear star formation – gas relation is able to reproduce the observed cosmic star formation history at $z \leqslant 10$.

on the metal enrichment in halos? The metallicity evolution is determined by the SFR (increases metal mass and decreases gas mass; Equation 12) and the gas accretion rate (increases gas mass and metal mass; Equation 4). Rearranging these equations it is easy to show (see appendix A) that the metallicity Z is constant, i.e., $\dot{Z} = 0$, if

$$r \equiv \frac{\dot{M}_{*,\rm form}}{\dot{M}_{\rm g,in}} = \frac{Z - Z_{\rm IGM}}{y(1-R)(1-\zeta)}. \qquad (20)$$

Given a SFR to gas accretion rate ratio r, the equilibrium metallicity is therefore

$$Z_{\rm eq}(r) = ry(1-R)(1-\zeta) + Z_{\rm IGM}. \qquad (21)$$

We demonstrate in appendix A that this equilibrium solution is (linearly) stable under most circumstances. Hence, for a given ratio r the metallicity of the ISM will increase or decrease until it reaches $Z_{\rm eq}(r)$. In other words, the competition between SFR and gas accretion rate drives the metallicity evolution in galaxies.

Equation (21) has a few interesting properties. First, it demonstrates that galactic outflows of warm/cold ISM material (parametrized by $\epsilon_{\rm out}$) play no role for the ISM metallicity. The reason is that while outflows carry metals away they also remove a corresponding amount of gas leaving the equilibrium metallicity unchanged. But since the metallicity of the ISM is likely close to $Z_{\rm eq}(r)$, it also remains unaffected. Second, $Z_{\rm eq}(r)$ depends only weakly on halo mass via ζ and, assuming $Z_{\rm IGM} = $ const, not on redshift. Hence, an analysis of the mass or redshift dependence of the metallicities of high redshift galaxies (combined with measured SFRs and mass accretion rates, estimated, e.g., from their halo masses) could be used to learn more about supernova driven outflows (parametrized by ζ) or the IGM enrichment ($Z_{\rm IGM}$).

In the next section, we study the connection between the star formation – gas relation and the driver of the metallicity evolution in galaxies, the ratio of SFR to gas accretion rate.

3.3 Gas Accretion and Star formation

Previously we have demonstrated that the functional form of the star formation – gas relation has a profound impact on the SFR of galaxies at high redshifts and we have attributed this effect to the altered metal enrichment. In this section, we will show that the metal enrichment is intrinsically linked to the star formation – gas relation via the balance between star formation and gas accretion in halos.

In Fig. 9 we plot the evolution of the ratio of the accretion time (gas mass divided by the gas accretion rate) to the gas depletion time (gas mass divided by SFR), i.e., the ratio of the SFR and the gas accretion rate, for halos of a range of masses. At $z \gtrsim 3$, a linear star formation – gas relation (Equations 13) results in a gas depletion time that is significantly longer (it is 2.5 Gyr if all gas is molecular and even longer otherwise) than the gas accretion time ($\sim 2-3 \times 10^7$ yr at $z = 30$, $\sim 1 - 2 \times 10^8$ yr at $z = 10$, $2 - 7 \times 10^8$ yr at $z = 5$). Hence, star formation is “depletion limited” at those redshifts. Changing the functional form of the star formation gas – relation alters the gas depletion times, but has only a small effect on the gas accretion rates, which are determined primarily by the mass accretion rates onto dark matter halos. A quadratic star formation gas – relation, for instance, results in gas depletion times as low as $\sim 2 \times 10^8$ yr at $z > 10$. As a consequence, star formation is “accretion limited” (the SFR is of the same order as the gas accretion rate) over most of cosmic history in this case.

Equation (20) allows us to understand the consequences of a depletion limited vs an accretion limited star formation. Consider a gas disk with a given metallicity Z. Such a gas

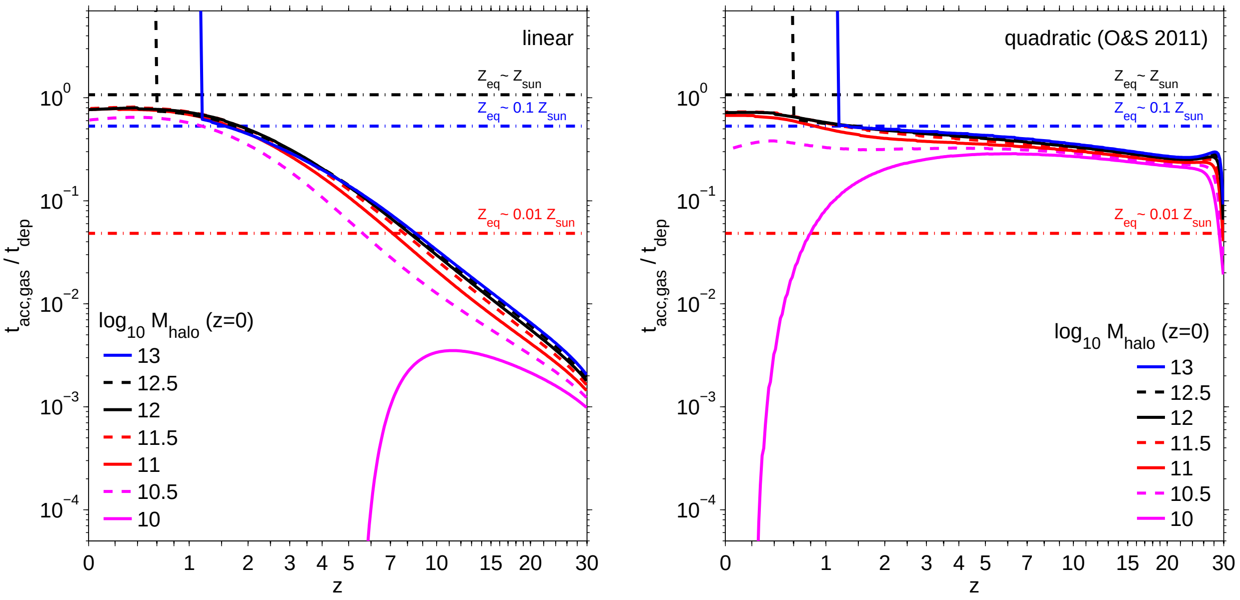

Figure 9. Ratio between gas accretion time (gas mass divided by gas accretion rate) and gas depletion time (gas mass divided by SFR), or equivalently the ratio between SFR and gas accretion rate, for galaxies in halos with present day masses in the range $10^{10} - 10^{13}$ $M_\odot$ (see legend). $\Sigma_{\rm SFR}$ is assumed to scale either linearly (left panel) or quadratically (right panel) with $\Sigma_{\rm H_2}$. Star formation is limited by gas accretion if the ratio is of the order of unity. The ratio gets very large in high mass halos at low redshift due to virial shock quenching of gas accretion, see Section 2). The dot-dashed lines shows the ratio of accretion to depletion time that is required to keep the gas metallicity constant at the value indicated in the figure. These lines are computed using Equation (20) with $\zeta = 0.9$ for $Z = 0.1 - 0.01$ $Z_\odot$ and $\zeta = 0.5$ for $Z = Z_\odot$. A ratio of accretion to depletion time above a given dot-dashed line with label Z indicates that metal enrichment via star formation outmatches the accretion of gas of low metallicity and, as a net effect, that the metallicity can raise above Z. A linear star formation – gas relation (Equation 13) has a gas depletion time that is significantly larger than the gas accretion time at $z > 3$. Metal enrichment and, hence, star formation is delayed until such times. In contrast, a quadratic star formation – gas relation has a depletion time that is short enough for star formation to catch up with the accretion rate early on. This leads to a fast and sustained enrichment to ~ 0.1 $Z_\odot$ at high redshift and, consequently, to high molecular fractions and substantial star formation over much of cosmic history.

disk will increase or decrease its metallicity until it matches the metallicity $Z_{\rm eq}$ specified by Equation (21) for the given SFR to gas accretion rate ratio r. For a stellar mass loss fraction of $R = 0.46$, a stellar metal yield of $y = 0.069$, and $\zeta = 0.9$ (true for all but the most massive halos at $z \sim 4 - 10$), we obtain $Z_{\rm eq} = 0.1$ $Z_\odot$ for $r = 0.53$, but $Z = 0.01$ $Z_\odot$ for $r = 0.048$. Therefore, if star formation is accretion limited the gas will get enriched to ~ 0.1 $Z_\odot$ or more on the gas accretion time scale. A rapid enrichment to $Z \sim 0.1$ $Z_\odot$ and accretion limited star formation has indeed been seen in many hydrodynamical simulations with a super-linear star formation model, see, e.g., Davé et al. (2006); Finlator et al. (2011). The equilibrium metallicity is small if r is small, i.e., if the depletion time is much longer than the gas accretion time. Hence, metal enrichment is delayed until $z \sim 2-3$ in case of a linear star formation – gas relation with a sufficiently large (>Gyr) depletion time.

To summarize, the functional form of the star formation – gas relation determines whether star formation in a given halo at a given time is depletion limited or accretion limited. This is crucial, because the evolution of the metallicity in a halo is driven by the competition between gas accretion and gas depletion (Equation 21). A linear star formation – gas relation delays metal enrichment until late times and, hence, suppresses star formation at high redshifts. In contrast, a strongly super-linear star formation – gas relation boosts metal enrichment and star formation at high redshifts.

A quantity similar to the ratio between SFR and gas accretion rate has been studied empirically by Behroozi et al. (2012a) using abundance matching techniques. In their work the baryon equivalent accretion rate (BEAR; $f_{\rm b}\dot{M}_{\rm halo}$) is used as a proxy for the unknown gas accretion rate. They find (see Fig. 1 in Behroozi et al. 2012a) that the SFR to BEAR ratio is roughly constant out to $z \sim 3$ and speculate that it might be a time-independent for much of cosmic history.

In Fig. 10 we show our predictions for the SFR to BEAR ratio using a similar color scheme and axis ranges as in Fig. 1 of Behroozi et al. (2012a). We compute baryon equivalent accretion rates based on the halo mass evolution formula provided in the appendix of Behroozi et al. (2012a). We find that a linear, H_2-based star formation gas – relation can reproduce their Fig. 1 reasonably well. Most importantly, the ratio between SFR and BEAR peaks around halo masses of $\sim 10^{11}$ $M_\odot$ at $z \lesssim 2$. Some features seen in Fig. 10, such as the complete lack of star formation in sufficiently low mass halos, may be related to the fact that the model follows the average evolution of galaxy properties and, at least in its current form, ignores the possibility of scatter caused by,

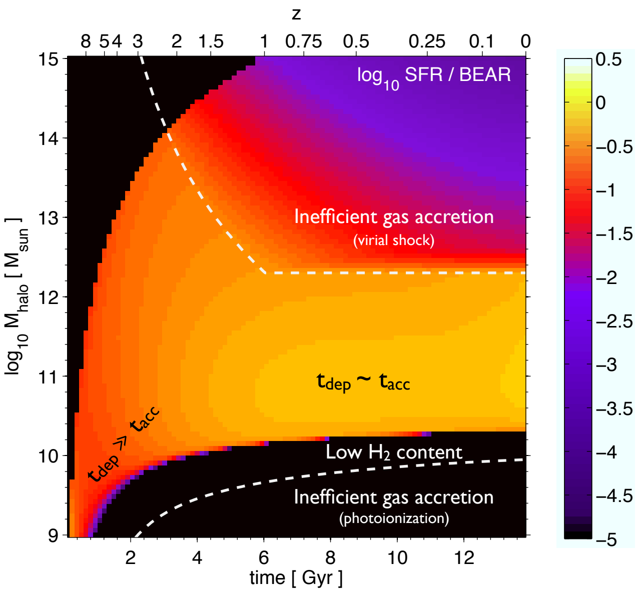

Figure 10. Ratio between SFR and baryon equivalent accretion rate ($f_b \dot{M}_{halo}$, BEAR) of galaxies as function of cosmic time and halo mass assuming a linear $\Sigma_{SFR} - \Sigma_{H_2}$ relation. For $z \lesssim 2$ the ratio peaks at a halo mass of approximately 10^{11} $M_\odot$ in reasonable agreement with observations (Behroozi et al. 2012a). Galaxies in low mass halos ($M_{halo} \lesssim 2 \times 10^{10}$ $M_\odot$ at $z \sim 0$) have their star formation quenched due the scarcity of molecular hydrogen in such halos. In addition, halos stop accreting gas once they become massive enough (the upper dashed line) to support a virial shock that prevents cold gas accretion onto the galaxy (Dekel & Birnboim 2006). At $z \lesssim 1$ star formation is confined to a narrow range of halo masses of approximately a few times 10^{10} $M_\odot$ to 10^{12} $M_\odot$ (Bouché et al. 2010; Krumholz & Dekel 2012).

e.g., the variability of the accretion rates or scatter in the disk sizes of galaxies.

3.4 An equilibrium view on galaxy evolution

Not only does the ratio between SFR and gas accretion rate regulate the metallicity in galaxies (see Equation 21), it also determines the gas fraction $f_g = M_g/M_{halo}$, stellar fraction $f_s = M_*/M_{halo}$, and the metal fraction $f_Z = M_Z/M_{halo}$ of galaxies.

Specifically, we can show using Equations 2, 3, 4, and 5 that for a given ratio $r \equiv \frac{\dot{M}_{*,form}}{\dot{M}_{g,in}}$

$\dot{f}_g = 0$ if $f_g = f_{g,eq}(r)$ with

$$f_{g,eq}(r) = [1 - r(1 - R + \epsilon_{out})]\, \epsilon_{in} f_{g,in} f_b, \qquad (22)$$

$\dot{f}_s = 0$ if $f_s = f_{s,eq}(r)$ with

$$f_{s,eq}(r) = (1 - f_{g,in}) f_b + \epsilon_{in} f_{g,in} f_b (1 - R) r, \qquad (23)$$

$\dot{f}_Z = 0$ if $f_Z = f_{Z,eq}(r)$ with

$$f_{Z,eq}(r) = Z_{eq}(r) f_{g,eq}(r), . \qquad (24)$$

The equilibrium values of other properties, such as the gas-to-stellar mass ratio $f_{gs} = f_g/f_s$ or the baron fraction $f_g + f_s$, can be obtained by combining these equations. For instance, $\dot{f}_{gs} = 0$ if $f_{gs} = f_{gs,eq}(r)$ with

$$f_{gs,eq}(r) = \frac{f_{g,eq}(r)}{f_{s,eq}(r)} = \frac{1 - (1 - R + \epsilon_{out}) r}{\frac{1 - f_{g,in}}{\epsilon_{in} f_{g,in}} + (1 - R) r}. \qquad (25)$$

We show in appendix A that the equilibrium state specified by Equations (22)-(24) is (linearly) stable under most circumstances for SFR to gas accretion rate ratios less than $1/(1 - R + \epsilon_{out})$. If, however, the galaxy is in a condition in which the H_2 fraction is extremely sensitive to small changes of the metal abundance of the ISM *and* star formation depends on the presence of molecular hydrogen, a run-away increase or decrease in H_2 abundance might take place. The latter ceases, and the galaxy reaches a new equilibrium, as soon as the H_2 fraction becomes sufficiently insensitive to changes in metal abundance. There can be no equilibrium state for $r > 1/(1 - R + \epsilon_{out})$, because it would lead to negative equilibrium gas fractions, see Equation 22. However, $r > 1/(1 - R + \epsilon_{out})$ is a physical possibility and applies, e.g., to massive galaxies at low redshifts that have their gas accretion quenched, but are still star forming. These galaxies are obviously not in an equilibrium state, but rely on their diminishing gas reservoir for star formation.

The stability of the equilibrium state implies, for instance, that if $f_g < f_{g,eq}(r)$ (and it is sufficiently close to the equilibrium value), the gas fraction increases and continues to do so until it reaches $f_{g,eq}(r)$. Similarly, if $f_g > f_{g,eq}(r)$, the gas fraction decreases until it matches the equilibrium value. We can therefore draw important conclusions for the gas fractions and gas-to-stellar mass ratios from Fig. 9. A small SFR to gas accretion rate ratio of, e.g., $r = 0.048$ corresponds to an equilibrium metallicity of $Z = 0.01$ $Z_\odot$, to an equilibrium gas fraction $f_{g,eq}/f_b \sim 0.83$ (0.46) and to an equilibrium gas-to-stellar mass ratio $f_{gs,eq} \sim 6.8$ (0.9). Here we assume[4] $f_{g,in} = 0.9$ ($f_{g,in} = 0.5$) and the default parameters of the model: $\epsilon_{in} = 1$, $R = 0.46$, $\epsilon_{out} = 1$. Hence, depletion limited star formation implies low metallicities, large gas fractions, and large gas-to-stellar mass ratios. In contrast, equilibrium metallicities are higher and equilibrium gas fractions and gas-to-stellar mass ratios are much lower if star formation is accretion limited. For instances, a SFR to gas accretion rate ratio $r = 0.53$ corresponds to $Z_{eq} = 0.1$ $Z_\odot$, $f_{g,eq}/f_b \sim 0.17$ (0.09) and $f_{gs,eq} \sim 0.46$ (0.14) for $f_{g,in} = 0.9$ ($f_{g,in} = 0.5$).

In the context of our model the baryonic properties of galaxies (of given halo mass and at a given redshift) are specified by f_Z, f_g, and f_s. In more abstract terms, the set (f_Z, f_g, f_s) represents the baryonic state of a galaxy. Equations (22) - (24) denote a curve[5] of fixed points parametrized by r in this baryonic state space. We demonstrate in the appendix that if (f_Z, f_g, f_s) is reasonably close to one of the fixed points it will approach it. As the cosmic accretion rate onto a halo changes, r changes as well and the galaxy transits smoothly from one equilibrium state to the next. Strong perturbations, such as major mergers, will also allow a galaxy to leave its current fixed point, but we would expect that such events are relatively rare. Hence, galaxy evolution is largely an evolution along this curve of fixed points driven by the external modulation of the gas accretion rate.

---

[4] The parameter $f_{g,in}$ can affect the predicted equilibrium gas fractions and gas-to-stellar mass ratios noticeably. The values chosen here are for illustration purposes, but we stress that we compute $f_{g,in}$ self-consistently in the model (see Section 2).

[5] This is only approximately true, because some of the terms in the Equations (22) - (24) dependent on more than just r, e.g., on the halo mass. This also implies that different galaxies will in general follow somewhat different curves of fixed points during their evolution. see Fig. 11

This clearly idealized picture assumes that galaxies can adapt on short timescales to changes in the SFR to gas accretion rate ratio r. The matter accretion time $M_{\rm halo}/\dot{M}_{\rm halo}$ is a natural timescale for gas fraction, stellar fractions, and metallicities to reach their equilibrium values, but the precise value depends on the parameters of the model, e.g., on the exponent of the star formation – gas relation, see appendix A. Given that the accretion time is of the order of the Hubble time at a given redshift, we expect that the stellar fractions, gas fractions and metallicities lag somewhat behind their equilibrium predictions, i.e., that gas fractions are somewhat underestimated by the equilibrium formalism, while stellar fractions and metallicities are overestimated. Fig. 11 confirms this point. Here, we show how halos evolve at redshift $z > 2$ in the $f_{\rm g}$-Z projection of the baryonic state space. We plot both the metallicities and gas fraction as computed by the model, and also the corresponding equilibrium quantities based on Equations (21) and (22). The equilibrium formalism describes the overall trend between $f_g - Z$ well, but for a given r it underpredicts the gas fractions and overpredicts the metallicities significantly. While properly correcting Equations (22) - (25) for the time lag is beyond the scope of this paper, we point out that the disagreement can be reduced if r is scaled by a factor $\sim 0.45[2-(2-n)^2]$ before applying Equations (21) and (22), see Fig. 11. Here, $n \in [1, 2]$ is the power-law exponent n of the star formation – gas relation.

We note that our equilibrium picture of galaxy formation differs from the "equilibrium condition" of a steady state model (Finlator & Davé 2008; Bouché et al. 2010; Dutton et al. 2010; Davé et al. 2012) in which the SFR in a given halo is balanced by the *net* gas accretion rate. Most importantly, we demonstrate that galaxies can be in a stable equilibrium even if the "equilibrium condition" is not even remotely satisfied. Specifically, galaxies can have little star formation and can massively build up their gas reservoirs and, yet, be in a proper equilibrium state. The reason is that the "equilibrium condition" of the steady state model is equivalent to the assumption that the gas *mass* in a galaxy remains constant. In contrast, we show that the actually stable equilibrium condition is that the gas *fraction* remains constant. The special equilibrium state with $r = 1/(1 - R + \epsilon_{\rm out})$ satisfies the "equilibrium condition" of the steady state model. Indeed a similar relation for r is often assumed to hold generally in the steady state approach, see e.g., Equation 2 of Davé et al. (2012). However, as Equation (22) shows the equilibrium gas fraction, and, hence, gas mass, in this equilibrium state is zero, and, hence, gas-rich, star forming galaxies at high redshift will not be in this particular state.

The equilibrium view presented in this section shows why metallicities, gas fractions, and stellar fractions of galaxies are strongly correlated. They are all coupled via a single parameter - the ratio between the SFR and the gas accretion rate, see Equations (22) - (24). Since the SFR depends on these galaxy properties, it follows that for a fixed functional form of the star formation – gas relation the evolution of global galaxy properties is regulated by just the gas accretion rate. Galactic outflows modify the equilibrium gas fractions (see Equation 22), but the primary regulator of star formation and other global galaxy properties is the gas accretion rate.

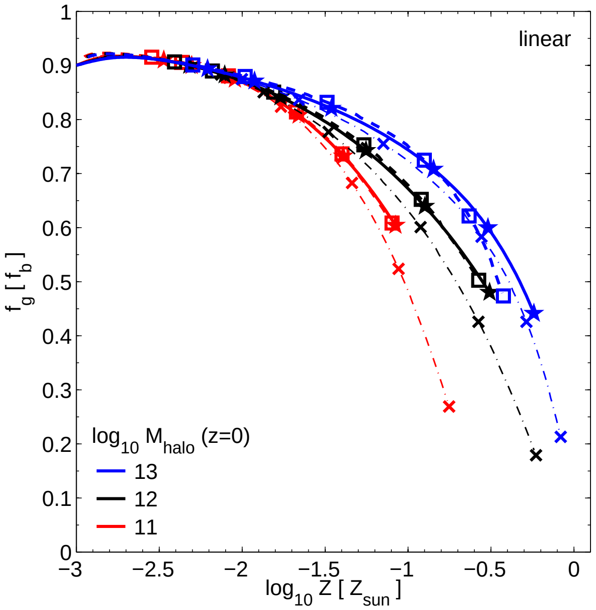

Figure 11. High redshift evolution of gas fractions and metallicites of halos with $z = 0$ masses of 10^{11} $M_\odot$ (red lines), 10^{12} $M_\odot$ (black lines), and 10^{13} $M_\odot$ (blue lines), respectively. The solid lines and stars show the evolution as predicted by the model presented in Section 2 for a linear $\Sigma_{\rm SFR} - \Sigma_{\rm H_2}$ relation. The dot-dashed lines and the crosses (dashed lines and squares) show the equilibrium predictions of Equations (21) and (22) with $r = \dot{M}_{*,\rm form}/\dot{M}_{\rm g,in}$ ($r = 0.45\,\dot{M}_{*,\rm form}/\dot{M}_{\rm g,in}$). Symbols show predictions at redshifts 10, 8, 6, 4, 3, and 2 (from top left to bottom right). The equilibrium ansatz predicts the right locus in the $f_{\rm g}$ vs Z plane, but for a given r underestimates $f_{\rm g}$ and overestimates Z. This disagreement is an indicator that galaxies have not sufficient time to fully reach the equilibrium solution. The simple rescaling of r by a factor $\sim 0.4 - 0.5$ improves the accuracy of the equilibrium formalism at $z \geqslant 2$.

3.5 Caveats

Our findings come with a number of potential caveats. First, our approach is based on the assumption that a single, unchanging star formation – gas relation, potentially parametrized by local galaxy properties such as the gas metallicity, or the free-fall time, etc., holds from early times until the present. Second, the model obviously idealizes many aspects of star formation in high redshift galaxies. For instance, it assumes that the gas is always arranged in an exponential disk (likely not true during major mergers)

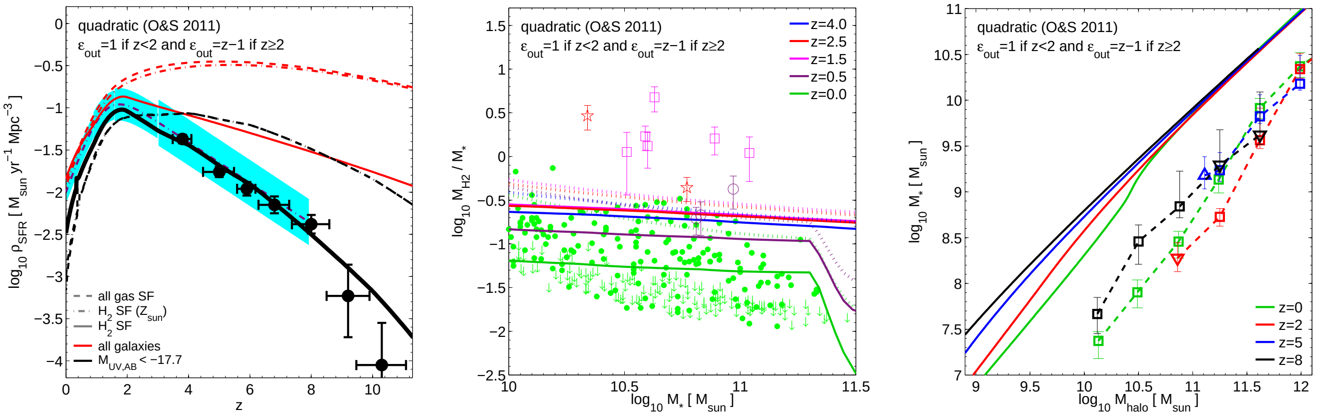

Figure 12. Predictions of an alternative model in which the mass ejection parameter $\epsilon_{\rm out}$ increases at $z > 2$. The star formation – gas relation is assumed to be quadratic (Equation 14). The panels show from left to right the cosmic star formation history, the gas-to-stellar mass ratio vs stellar mass, and the relation between stellar mass and halo mass. The lines and symbols are as in Fig. 4, Fig. 2, and Fig. 3 for the left, middle, and right panel, respectively. The ad-hoc scaling of $\epsilon_{\rm out}$ with redshift cures the excess of SFRDs at high z otherwise predicted for a quadratic star formation – gas relation, see Fig. 6. However, it does not help in bringing the $M_{\rm halo} - M_*$ relation or the gas-to-stellar mass fractions in agreement with observations.

and that accreted halos donate all their cold gas to the central galaxy. Furthermore, since the model only makes predictions for the mean evolution of halos of a given mass, it ignores variations in the accretion histories and possible environmental dependences. Such, admittedly interesting, complexities are best studied in numerical simulations. However, demanding requirements in terms of simulation volume and resolution (see Schaye et al. 2010 for a resolution study) limit the systematic exploration of the parameter space of feedback and star formation models using this approach. Nonetheless, we plan to compare the predictions of our model with dedicated high resolution cosmological simulations in future work.

Additional caveats are:

- *Model parameters:* We use the same set of parameters as in Krumholz & Dekel (2012). Most of these parameters have a theoretical or empirical justification (we refer to reader to Krumholz & Dekel 2012). When we vary the model parameters within their justifiable ranges, we find that the mass ejection rate into the IGM per SFR, $\epsilon_{\rm out}$, the metallicity of the IGM, $Z_{\rm IGM}$, and the spin of the halo, λ, have the largest effect on the predicted cosmic star formation history. The impact of these changes is largest if a linear star formation – gas relation is used, and smaller if the relation is highly non-linear and, hence, star formation is accretion limited early on. However, even for a linear relation we can vary each of these parameters by a factor of ~ 3 without any qualitative changes in the model predictions. For instance, increasing $\epsilon_{\rm out}$ by such a factor decreases the SFRD at $z \sim 1-2$ by ~ 0.5 dex, but leads to little change at higher redshifts (e.g., at $z = 4$ the decrease in the SFRD is only 0.2 dex). Reducing $Z_{\rm IGM}$ by a factor 3 delays star formation in low mass halos and results in SFRDs that are reduced by a similar factor. Decreasing λ from 0.07 to 0.05 increases the SFRD at $z \sim 4-10$ by a factor $\sim 2-3$. The predicted *observable* cosmic star formation history is less affected ($\lesssim 0.2$ dex typically).

- *Missing physics:* Given the simplicity of the model it is possible that we are missing an important physical process that would affect the model predictions and potentially change our conclusions. For instance, a mechanism that increases the mass ejection rate of the winds with redshift would help to mitigate some of the problems of a highly non-linear star formation – gas relation. We demonstrate this in Fig. 12 where we show the model predictions for a hypothetical scenario in which $\epsilon_{out} = 1$ for $z < 2$ and $\epsilon_{out} = z - 1$ for $z \geqslant 2$. Clearly, by choosing the scaling of ϵ_{out} properly even a quadratic star formation – gas relation can be brought into agreement with observations of the cosmic star formation history. However, this does not necessarily mean that other observational constraints are met as well. The figure shows, for instance, that this particular model fails in reproducing the $M_{\rm halo} - M_*$ relation at any redshift and the gas-to-stellar mass ratios at $z \gtrsim 1$. In contrast, a simple, linear star formation – gas relation with an $\mathrm{H_2}$ depletion time of 2.5 Gyr (as observed in the local universe) does not require the assumption of additional ad-hoc (and fine-tuned) physics to reproduce global galaxy properties from high redshifts until today, see Section 3.1.

- *Metal mixing*: We assume that metals in the disks of galaxies are efficiently mixed, i.e., that the gas has a spatially uniform metallicity. In reality, we expect some metallicity gradients, since accretion of metal-poor gas occurs preferentially at the outer edge of the disk. Numerical simulation by Kuhlen et al. (2012) indicate that the metallicity difference is only modest for the majority of the gas in the disks of high redshift galaxies. In order to test the importance of metal mixing we modified the model to allow only local enrichment (i.e., metals produced in a given radius bin are added only to that radial bin). This somewhat extreme case of no-mixing lowers the predicted SFRDs by ~ 3 if we use a linear star formation – gas relation, but makes almost no difference if the relation is strongly non-linear.

- *Dust:* The model assumes that the dust-to-gas ratio (which determines the H_2 abundance) scales proportional to the metallicity. At low metallicities ($Z < 0.1Z_\odot$) it is unclear whether this assumption is justified. A potential concern is that at high z the dust production may lag behind the metal production, limiting the formation of H_2, and thus star formation. Empirically, there is evidence for a substantial presence of dust in high redshift galaxies from absorption line studies of damped Ly-α systems at $z \sim 1.5-3.5$ (e.g., Pettini et al. 1994; Prochaska & Wolfe 2002) and from the thermal emission of dust in quasar hosts at $z \sim 4-6$ (e.g., Omont et al. 2001; Bertoldi & Cox 2002). Both AGB stars (e.g., Valiante et al. 2009) and supernovae (e.g., Todini & Ferrara 2001) have been proposed as formation channels for dust at such high redshifts. If supernovae dominate the dust production, we expect a dust production time scale of $\sim 10^7$ yr, which is shorter than the gas accretion time ($\sim 1-2\times10^8$ at $z=10$) and, hence, not a limiting factor.

- *Molecular hydrogen:* The H_2 abundances are estimated based on the equilibrium model by Krumholz et al. (2009a). For Milky-Way like, turbulent ISM conditions the H_2 formation times $t_{\rm H_2,form}$ are short ($\sim 10^6$ yr, Glover & Mac Low 2007), but they could be higher in high redshift galaxies. With $t_{\rm H_2,form} \propto (Z\rho)^{-1}$ (Hollenbach et al. 1971) and gas densities in the high z galaxies that are likely an order of magnitude higher than in the Milky Way, we expect formation times of $\lesssim 10^8$ yr for gas with metallicities $Z \geqslant 2\times10^{-5}$, which is sufficiently short to not limit star formation. In addition, numerical simulations of star formation in the ISM show that decreasing the metallicity from solar to a hundredth solar postpones the onset of star formation only by a few Myr (Glover & Clark 2012). Hence, we do not expect that star formation is limited by the H_2 formation time even in case of a highly non-linear star formation – gas relation.

4 SUMMARY AND DISCUSSION

We have studied the implications of the functional form of the star formation – gas relation for the cosmic star formation history, for gas accretion in galaxies, and for the evolution of global galaxy properties using a model that follows the average evolution of galaxies in growing dark matter halos across cosmic time (Krumholz & Dekel 2012). We specifically contrasted the predictions for a linear star formation – gas relation (Bigiel et al. 2011) with those for a quadratic relation (Ostriker & Shetty 2011), but also tested a few other functional forms suggested in the literature (Krumholz et al. 2009b, 2012; Shetty et al. 2012). Our main findings are as follows:

- We show that a linear $\Sigma_{\rm SFR} - \Sigma_{\rm H_2}$ relation with a ~ 2.5 Gyr depletion time results in a mass – metallicity relation, in gas-to-stellar mass ratios, and in a stellar-to-halo mass relation that is in reasonable agreement with observations.
- The functional form of the star formation – gas relation strongly affects the cosmic star formation history at $z \gtrsim 4$. A linear star formation – H_2 relation suppresses star formation in halos with $z=0$ masses below $\sim 10^{11}$ $M_\odot$. If, however, the star formation – gas relation is highly non-linear, star formation can occur in halos with $z=0$ masses even below $\sim 10^{10}$ $M_\odot$. As a result, SFRDs can differ by factors of ~ 30 at $z=10$ (~ 5 at $z=6$), see Fig. 4 and 6, between the linear and the quadratic star formation – H_2 relation.
- The star formation – gas relation has a similar effect on the *observable* cosmic star formation history, i.e., the SFRD of galaxies with magnitudes accessible to observations (here assumed to be $M_{\rm UV,AB} < -17.7$, Bouwens et al. 2012b). A linear star – H_2 formation relation results in an observable cosmic star formation history compatible with observational data, while a quadratic relation strongly overpredicts the observable SFRDs at high redshift.
- Whether star formation is based on H_2 or on total gas leaves little imprint on the observable cosmic star formation history. There is also little difference in the full (including all galaxies) cosmic star formation history if the star formation – gas relation is highly super-linear. If the relation is linear, however, the choice of H_2-based vs total gas based star formation affects the SFRD at high redshift, e.g, by more than an order of magnitude at $z=8$.
- For the adopted linear $\Sigma_{\rm SFR} - \Sigma_{\rm H_2}$ relation (Equation 13), the gas depletion time exceeds the gas accretion time ($\sim$ free-fall time of the halo) at high z. During this time the SFRs are orders of magnitude smaller than the gas accretion rates. Star formation becomes accretion limited, i.e., SFRs $\sim$ gas accretion rates, only at relatively recent epochs ($z \lesssim 2-3$). We show that these predictions are in reasonable agreement with abundance matching predictions by Behroozi et al. (2012a). In contrast, star formation is close to accretion limited already at very high redshifts if the star formation – gas relation is quadratic.
- The evolution of metallicities, gas fractions, and stellar fractions are driven by the ratio r between the SFR and gas accretion rate. In fact, given a star formation – gas relation galaxies evolve towards a (linearly stable) equilibrium state with gas fraction, stellar fraction and metallicity determined only by the gas accretion rate. The equilibrium concept presented in this work differs from the steady state model suggested in the literature (e.g., Davé et al. 2012) and shows that galaxies can be in equilibrium even if their gas masses are growing quickly. We argue that galaxy evolution can be interpreted as an evolution along a set of equilibria driven primarily by the change in the cosmic accretion rate.

As pointed out above we find that the observed cosmic star formation history is well reproduced if the star formation – gas relation is linear and has an H_2 depletion time of ~ 2.5 Gyr. Given the simplicity of the model and the uncertainties in the observational data we do not rule out the possibility that the relation is actually slightly super- or sub-linear (e.g., has an exponent in the range $\sim 0.85-1.3$) or has a somewhat different depletion time. However, our findings are difficult to reconcile with the idea of a highly super-linear, especially quadratic, star formation – gas relation.

Many of our findings for a *linear* star formation – gas relation are almost identical to those found by Krumholz & Dekel (2012) for a *non-linear* star formation – gas relation, similar to Equation 16, with an exponent of 1.33 at high gas surface densities. However, their star formation – gas relation uses a very large transition surface density

($\Sigma_{\rm g} = 850\ M_\odot$ pc^{-2} compared with $\Sigma_{\rm g} = 85\ M_\odot$ pc^{-2} of Equation 16) at which the scaling changes from sub-linear to super-linear. This matters because gas surface densities of high redshift galaxies are of the order of a few 100 $M_\odot$ pc^{-2}, see Fig. 7. Hence, a transition surface density as large as $\Sigma_{\rm g} = 850\ M_\odot$ pc^{-2} implies that a large fraction of the gas in galaxy disks is subject to a sub-linear star formation – gas relation and that $\Sigma_{\rm SFR}$ scales super-linearly with $\Sigma_{\rm H_2}$ only in the central regions (where surface densities are larger by a factor $e^{1.7} \sim 5.5$ than the surface densities at the half-mass radius). Averaging over sub- and super-linear regions results in a close-to-linear relation between H$_2$ masses and SFRs in galaxies, hence, to similar predictions as for the strictly linear star formation – gas relation given by Equation (13).

Krumholz & Dekel (2012) argue that star formation based on H$_2$ is an essential ingredient to bring the predicted SFRDs at high redshifts in agreement with observations. We find that metal-dependent quenching of star formation based on H$_2$ has only a small impact (0.3 dex at $z \sim 9$ and less at lower redshift) on the *observable* SFRDs at high redshift, because it affects primarily faint galaxies below the current detection limits. However, metal-dependent quenching plays an important role for the total (i.e., including galaxies below the detection limits) SFRD *if* the star formation – gas relation is not highly super-linear. This is in agreement with Krumholz & Dekel (2012) who effectively use an approximately linear star formation – gas relation (see above) to study the total SFRD. In case of a strongly super-linear relation, however, star formation in galaxies is almost always close to being accretion limited even at $z \sim 10$. Therefore, galaxies get enriched early on and SFRs proceed at a rate that is effectively identical (to within a factor of 2 or so) to the gas accretion rates, independently on whether a $\Sigma_{\rm SFR} - \Sigma_{\rm H_2}$ or a $\Sigma_{\rm SFR} - \Sigma_{\rm g}$ relation is used.

Schaye et al. (2010) analyze the star formation history of the universe with large scale cosmological simulations and find little evidence for a change of the (total) cosmic star formation rate with metallicity. The star formation in their simulations is modeled via a moderately non-linear "Schmidt law", i.e., a star formation – gas relation based on volumetric densities. They allow star formation only in regions with densities above a threshold that is either fixed (the default model) or scales with metallicity. However, their threshold is much lower than the density required for H$_2$ formation (Gnedin & Kravtsov 2011) and the metallicity scaling much weaker ($\propto \log Z^{-1}$, Schaye 2004) than the one expected to regulate the presence of H$_2$ (approximately $\propto Z^{-1}$, see Equations 8–11). It is therefore difficult to properly judge the implications of their findings in the context of H$_2$ based star formation.

Kuhlen et al. (2012) study the evolution of the cosmic star formation history in simulations that follow the abundance of H$_2$ directly (using Equations 8–11) and compare these to simulations that use a fixed density threshold for star formation. The chosen threshold (50 cm^{-3}) corresponds approximately to the transition from atomic to molecular phase for gas of solar metallicity. The Schmidt law used in the simulations is moderately non-linear. Hence, we would expect that the two sets of simulations result in very similar predictions for the SFRs of galaxies bright enough to be observable. Indeed, Kuhlen et al. (2012) find that the SFRDs of galaxies with stellar masses larger than $10^{7.75}\ M_\odot$ change by (only) a factor of ~ 2. The differences are even smaller when galaxies are selected based on their UV luminosity ($M_{\rm UV,AB} < -17.7$; M. Kuhlen private communication).

Another interesting question is the importance of stellar feedback for the regulation of star formation at high z. Schaye et al. (2010) found that increasing the exponent of the star formation – gas relation or decreasing the depletion time has little impact on the cosmic star formation history at $z \lesssim 6$ and the authors use this fact to infer that galaxies are able to regulate their star formation via feedback processes. However, their default star formation – gas relation is non-linear and, hence, increasing its exponent or decreasing its depletion time further has little impact if SFRs are already close to the accretion limit. We also argue, based on the equilibrium view of galaxy evolution presented in Section 3.4, against the interpretation that star formation is regulated by large scale galactic outflows, because *for a given star formation – gas relation* the gas accretion rate (or the matter accretion rate onto the halo) is the main regulatory mechanism of star formation. Of course, star formation may be feedback-regulated within the ISM. In particular, the existence of a star formation – gas relation that holds on $\sim$ kpc scales may be a consequence of the interplay between turbulence, gravity, and feedback in the first place (e.g., Hopkins et al. 2011).

REFERENCES

Barnes J., Efstathiou G., 1987, ApJ, 319, 575

Behroozi P. S., Wechsler R. H., Conroy C., 2012a, ArXiv e-prints

Behroozi P. S., Wechsler R. H., Conroy C., 2012b, ArXiv e-prints

Bertoldi F., Cox P., 2002, A&A, 384, L11

Bigiel F., Blitz L., 2012, ApJ, 756, 183

Bigiel F., Leroy A., Walter F., Brinks E., de Blok W. J. G., Madore B., Thornley M. D., 2008, AJ, 136, 2846

Bigiel F. et al., 2011, ApJ, 730, L13

Bouché N. et al., 2010, ApJ, 718, 1001

Bouwens R. et al., 2012a, ArXiv e-prints

Bouwens R. J., Illingworth G. D., Franx M., Ford H., 2007, ApJ, 670, 928

Bouwens R. J. et al., 2012b, ApJ, 754, 83

Bullock J. S., Dekel A., Kolatt T. S., Kravtsov A. V., Klypin A. A., Porciani C., Primack J. R., 2001, ApJ, 555, 240

Chabrier G., 2005, in Astrophysics and Space Science Library, Vol. 327, The Initial Mass Function 50 Years Later, Corbelli E., Palla F., Zinnecker H., eds., p. 41

Daddi E. et al., 2010a, ApJ, 713, 686

Daddi E. et al., 2010b, ApJ, 714, L118

Davé R., Finlator K., Oppenheimer B. D., 2006, MNRAS, 370, 273

Davé R., Finlator K., Oppenheimer B. D., 2012, MNRAS, 421, 98

Dekel A., Birnboim Y., 2006, MNRAS, 368, 2

Dekel A. et al., 2009, Nature, 457, 451

Dutton A. A., van den Bosch F. C., Dekel A., 2010, MNRAS, 405, 1690

Dutton A. A. et al., 2011, MNRAS, 410, 1660

Erb D. K., 2008, ApJ, 674, 151

Erb D. K., Shapley A. E., Pettini M., Steidel C. C., Reddy N. A., Adelberger K. L., 2006, ApJ, 644, 813

Feldmann R., Gnedin N. Y., Kravtsov A. V., 2011, ApJ, 732, 115

Feldmann R., Gnedin N. Y., Kravtsov A. V., 2012, ApJ, 758, 127

Finlator K., Davé R., 2008, MNRAS, 385, 2181

Finlator K., Oppenheimer B. D., Davé R., 2011, MNRAS, 410, 1703

Gao Y., Solomon P. M., 2004, ApJ, 606, 271

Genzel R. et al., 2010, MNRAS, 407, 2091

Glover S. C. O., Clark P. C., 2012, MNRAS, 426, 377

Glover S. C. O., Mac Low M.-M., 2007, ApJ, 659, 1317

Gnedin N. Y., Kravtsov A. V., 2010, ApJ, 714, 287

Gnedin N. Y., Kravtsov A. V., 2011, ApJ, 728, 88

Gnedin N. Y., Tassis K., Kravtsov A. V., 2009, ApJ, 697, 55

Heyer M. H., Corbelli E., Schneider S. E., Young J. S., 2004, ApJ, 602, 723

Hoeft M., Yepes G., Gottlöber S., Springel V., 2006, MNRAS, 371, 401

Hollenbach D. J., Werner M. W., Salpeter E. E., 1971, ApJ, 163, 165

Hopkins P. F., Cox T. J., Hernquist L., Narayanan D., Hayward C. C., Murray N., 2012, ArXiv e-prints

Hopkins P. F., Quataert E., Murray N., 2011, MNRAS, 417, 950

Kennicutt, Jr. R. C., 1989, ApJ, 344, 685

Kennicutt, Jr. R. C., 1998, ApJ, 498, 541

Kewley L. J., Ellison S. L., 2008, ApJ, 681, 1183

Klypin A. A., Trujillo-Gomez S., Primack J., 2011, ApJ, 740, 102

Komatsu E. et al., 2011, ApJS, 192, 18

Krumholz M. R., Dekel A., 2012, ApJ, 753, 16

Krumholz M. R., Dekel A., McKee C. F., 2012, ApJ, 745, 69

Krumholz M. R., McKee C. F., 2005, ApJ, 630, 250

Krumholz M. R., McKee C. F., Tumlinson J., 2008, ApJ, 689, 865

Krumholz M. R., McKee C. F., Tumlinson J., 2009a, ApJ, 693, 216

Krumholz M. R., McKee C. F., Tumlinson J., 2009b, ApJ, 699, 850

Krumholz M. R., Thompson T. A., 2007, ApJ, 669, 289

Kuhlen M., Faucher-Giguère C.-A., 2012, MNRAS, 423, 862

Kuhlen M., Krumholz M. R., Madau P., Smith B. D., Wise J., 2012, ApJ, 749, 36

Lada C. J., Forbrich J., Lombardi M., Alves J. F., 2012, ApJ, 745, 190

Leroy A. K. et al., 2011, ApJ, 737, 12

Lilly S. J., Le Fevre O., Hammer F., Crampton D., 1996, ApJ, 460, L1

Liu G., Koda J., Calzetti D., Fukuhara M., Momose R., 2011, ApJ, 735, 63

Madau P., Ferguson H. C., Dickinson M. E., Giavalisco M., Steidel C. C., Fruchter A., 1996, MNRAS, 283, 1388

Magdis G. E. et al., 2012a, ApJ, 760, 6

Magdis G. E. et al., 2012b, ApJ, 758, L9

Maiolino R. et al., 2008, A&A, 488, 463

Mo H. J., Mao S., White S. D. M., 1998, MNRAS, 295, 319

Mo H. J., White S. D. M., 2002, MNRAS, 336, 112

Moustakas J., Kennicutt, Jr. R. C., Tremonti C. A., Dale D. A., Smith J.-D. T., Calzetti D., 2010, ApJS, 190, 233

Narayanan D., Bothwell M., Davé R., 2012a, MNRAS, 426, 1178

Narayanan D., Cox T. J., Hayward C. C., Hernquist L., 2011, MNRAS, 412, 287

Narayanan D., Krumholz M. R., Ostriker E. C., Hernquist L., 2012b, MNRAS, 421, 3127

Navarro J. F., Frenk C. S., White S. D. M., 1997, ApJ, 490, 493

Neistein E., Dekel A., 2008, MNRAS, 383, 615

Neistein E., van den Bosch F. C., Dekel A., 2006, MNRAS, 372, 933

Oesch P. A. et al., 2012, ApJ, 745, 110

Okamoto T., Gao L., Theuns T., 2008, MNRAS, 390, 920

Omont A., Cox P., Bertoldi F., McMahon R. G., Carilli C., Isaak K. G., 2001, A&A, 374, 371

Ostriker E. C., McKee C. F., Leroy A. K., 2010, ApJ, 721, 975

Ostriker E. C., Shetty R., 2011, ApJ, 731, 41

Pettini M., Smith L. J., Hunstead R. W., King D. L., 1994, ApJ, 426, 79

Prada F., Klypin A. A., Cuesta A. J., Betancort-Rijo J. E., Primack J., 2012, MNRAS, 423, 3018

Prochaska J. X., Wolfe A. M., 2002, ApJ, 566, 68

Rahman N. et al., 2011, ApJ, 730, 72

Rahman N. et al., 2012, ApJ, 745, 183

Reyes R., Mandelbaum R., Gunn J. E., Nakajima R., Seljak U., Hirata C. M., 2012, MNRAS, 425, 2610

Robertson B. E., Kravtsov A. V., 2008, ApJ, 680, 1083

Rodighiero G. et al., 2011, ApJ, 739, L40

Saintonge A. et al., 2011, MNRAS, 415, 32

Schaye J., 2004, ApJ, 609, 667

Schaye J. et al., 2010, MNRAS, 402, 1536

Schmidt M., 1959, ApJ, 129, 243

Schmidt M., 1963, ApJ, 137, 758

Schruba A., Leroy A. K., Walter F., Sandstrom K., Rosolowsky E., 2010, ApJ, 722, 1699

Shetty R., Kelly B. C., Bigiel F., 2012, ArXiv e-prints

Steidel C. C., Adelberger K. L., Giavalisco M., Dickinson M., Pettini M., 1999, ApJ, 519, 1

Tacconi L. J. et al., 2010, Nature, 463, 781

Tacconi L. J. et al., 2012, ArXiv e-prints

Todini P., Ferrara A., 2001, MNRAS, 325, 726

Tremonti C. A. et al., 2004, ApJ, 613, 898

Valiante R., Schneider R., Bianchi S., Andersen A. C., 2009, MNRAS, 397, 1661

Walter F., Brinks E., de Blok W. J. G., Bigiel F., Kennicutt, Jr. R. C., Thornley M. D., Leroy A., 2008, AJ, 136, 2563

Wise J. H., Turk M. J., Norman M. L., Abel T., 2012, ApJ, 745, 50

Wong T., Blitz L., 2002, ApJ, 569, 157

Zaritsky D., Kennicutt, Jr. R. C., Huchra J. P., 1994, ApJ, 420, 87

ACKNOWLEDGMENTS

I would like to thank Peter Behroozi, Claude-André Faucher-Giguère, Michael Kuhlen, and Matt McQuinn for insightful discussions regarding H_2-based star formation in dwarf galaxies, the suppression of accretion due to a photoionizing background, and abundance matching techniques. I am also grateful to Nick Gnedin and Michael Kuhlen for helpful comments on an early draft of this paper. I acknowledge support for this work by NASA through Hubble Fellowship grant HF-51304.01-A awarded by the Space Telescope Science Institute, which is operated by the Association of Universities for Research in Astronomy, Inc., for NASA, under contract NAS 5-26555. This work made extensive use of the NASA Astrophysics Data System and `arXiv.org` preprint server.

APPENDIX A: EQUILIBRIA AND STABILITY ANALYSIS

The time derivatives of the metallicity Z, metal fraction f_Z, gas fraction f_g, and stellar fraction f_s are

$$\dot{Z} = \frac{d}{dt}\frac{M_Z}{M_g} = \frac{1}{M_g}\left(\dot{M}_Z - Z\dot{M}_g\right), \tag{A1}$$

$$\dot{f_X} = \frac{d}{dt}\frac{M_X}{M_h} = \frac{1}{M_h}\left(\dot{M}_X - f_X\dot{M}_h\right) \equiv g_X(f_Z, f_g, f_s), \tag{A2}$$

here $X \in \{Z, g, s\}$ and we introduced the functions g_Z, g_g, and g_s.

Combining Equation (A1) with Equations (4) and (12) we obtain

$$\begin{aligned}\dot{Z} &= \frac{1}{M_g}\left[y(1-R)(1-\zeta)\dot{M}_{*,\mathrm{form}} - (Z - Z_{\mathrm{IGM}})\dot{M}_{\mathrm{g,in}}\right] \\ &= \frac{\dot{M}_{\mathrm{g,in}}}{M_g}\left[y(1-R)(1-\zeta)r - (Z - Z_{\mathrm{IGM}})\right].\end{aligned} \tag{A3}$$

The second equality assumes $\dot{M}_{\mathrm{g,in}} \neq 0$ and we introduced $r = \dot{M}_{*,\mathrm{form}}/\dot{M}_{\mathrm{g,in}}$. Clearly, aside from trivial cases such as $\dot{M}_{*,\mathrm{form}} = 0$ *and* $Z = Z_{\mathrm{IGM}}$, the metallicity can only be constant if the equilibrium condition (20,21) is satisfied, i.e, for $Z_{\mathrm{eq}} = y(1-R)(1-\zeta)r + Z_{\mathrm{IGM}}$.

Let us assume that the metallicity is perturbed slightly relative to its equilibrium value, i.e., $Z = Z_{\mathrm{eq}} + \delta$ with a small perturbation δ. Let us also introduce the shorthands $A = 1 - R + \epsilon_{\mathrm{out}}$, $B = y(1-R)(1-\zeta)$, $C = \epsilon_{\mathrm{in}} f_{\mathrm{g,in}} f_{\mathrm{b}}$, $D = (1 - f_{\mathrm{g,in}})f_{\mathrm{b}}$ to simplify the notation. The evolution of δ can be obtained from the linearized version of Equation (A3).

$$\dot{\delta} = \delta\,\frac{\dot{M}_{\mathrm{g,in}}}{M_g}\left[B\frac{\partial r}{\partial Z}(Z_{\mathrm{eq}}) - 1\right]. \tag{A4}$$

Hence, we find that $\delta \to 0$ if $B\frac{\partial r}{\partial Z} < 1$. In particular, if, for a given gas configuration, star formation proceeds independently of its metallicity, the equilibrium metallicity is always stable against perturbations. However, if the SFR changes strongly with metallicity the equilibrium can become unstable. In this case the perturbation initially grows, i.e., gas is enriched or depleted, but eventually $\frac{\partial r}{\partial Z}$ becomes small (e.g., when all the gas is molecular) and the system approaches a new equilibrium. We note that this derivation ignores changes to the gas masses (or stellar masses), and hence, it does not prove that Z_{eq} is the metallicity of an equilibrium state that is also stable against these perturbations, which is what we show next.

Consider a galaxy that resides in a halo with mass M_{halo} and that accretes gas and stars according to the Equations (4) and (5). The accretion rates are governed by gravitation and not affected by changes in the gas fraction or the metallicity of the galaxy. Also, the scale radius of the gas disk (proportional to the virial radius of the halo) is not affected by such changes (at least in the context of the model of Section 2). We assume that the star formation in the galaxy is described by a power-law relationship

$$M_{*,\mathrm{form}} = N\left[f_g f_{\mathrm{H}_2}(f_Z)\right]^n. \tag{A5}$$

Here, N is a normalization constant (which includes everything that does not change when the gas fraction or metal fraction changes) and n is the power-law exponent of the star formation – gas relation. The assumption that the H_2 fraction of the gas depends on f_Z and not on Z deserves a comment. Equation (8) shows that the H_2 fraction depends primarily on the dust optical depth (Equation 11). The latter is proportional to $Z\Sigma_{\mathrm{g}} \propto f_Z$.

Let $f_X = f_{X,\mathrm{eq}} + \delta_X$ be a small perturbation around the equilibrium state $(f_{Z,\mathrm{eq}}, f_{g,\mathrm{eq}}, f_{s,\mathrm{eq}})$ (see Equations 22 and 25). The evolution of the perturbation is governed by the following system of equations

$$\begin{aligned}\dot{f_X} = \dot{\delta_X} &= g_X(f_Z, f_g, f_s) \\ &\approx \sum_{Y \in \{Z,g,s\}} \delta_Y \frac{\partial g_X}{\partial f_Y}(f_{Z,\mathrm{eq}}, f_{g,\mathrm{eq}}, f_{s,\mathrm{eq}}).\end{aligned}$$

If all eigenvalues of the Jacobian $J_{X,Y} = \frac{\partial g_X}{\partial f_Y}$ have a real value less than zero, then a system in the state $(f_{Z,\mathrm{eq}}, f_{g,\mathrm{eq}}, f_{s,\mathrm{eq}})$ is stable against small perturbations.

In the following we use the additional shorthands $E =$

$\frac{\partial \ln f_{\rm H_2}}{\partial \ln f_Z}(f_{Z,\rm eq})$ and $T = M_{\rm halo}/\dot{M}_{\rm halo}$. We find that

$$J_{Z,Z} = \frac{1}{T}\left[(f_{Z,\rm eq} - CZ_{\rm IGM})\left(\frac{nE}{f_{Z,\rm eq}} - \frac{A}{Bf_{g,\rm eq} - Af_{Z,\rm eq}}\right) - 1\right]$$
$$J_{Z,g} = \frac{1}{T}(f_{Z,\rm eq} - CZ_{\rm IGM})\left[\frac{n}{f_{g,\rm eq}} + \frac{f_{Z,\rm eq}}{f_{g,\rm eq}}\frac{A}{Bf_{g,\rm eq} - Af_{Z,\rm eq}}\right]$$
$$J_{Z,s} = 0$$
$$J_{g,Z} = -\frac{1}{T}\left[\frac{nE}{f_{Z,\rm eq}}(C - f_{g,\rm eq})\right]$$
$$J_{g,g} = -\frac{1}{T}\left[\frac{n}{f_{g,\rm eq}}(C - f_{g,\rm eq}) + 1\right]$$
$$J_{g,s} = 0$$
$$J_{s,Z} = \frac{1}{T}\left[\frac{nE}{f_{Z,\rm eq}}(f_{s,\rm eq} - D)\right]$$
$$J_{s,g} = \frac{1}{T}\frac{n}{f_{g,\rm eq}}(f_{s,\rm eq} - D)$$
$$J_{s,s} = -\frac{1}{T}.$$

Replacing $(f_{Z,\rm eq}, f_{g,\rm eq}, f_{s,\rm eq})$ with the expressions (22) – (24) allows us to write $J_{X,Y}$ as a function of the following parameters: n, A, B, E, $Z_{\rm IGM}$, and r, the ratio between SFRs and gas accretion rate, *for the given equilibrium state*. In particular, C and D drop out, which shows that the stability of the equilibrium does not depend on the values of $f_{\rm g,in}$ or $\epsilon_{\rm in}$.

$$J_{Z,Z} = \frac{1}{T}\left[\frac{nEBr^2A + (nEZ_{\rm IGM}A + B - nEB)r + Z_{\rm IGM}}{(Br + Z_{\rm IGM})(Ar-1)}\right]$$
$$J_{Z,g} = \frac{1}{T}\left[r\frac{(nBA - BA)r - nB + nZ_{\rm IGM}A - Z_{\rm IGM}A}{Ar-1}\right]$$
$$J_{Z,s} = 0$$
$$J_{g,Z} = \frac{1}{T}\left[\frac{nEAr}{(Br + Z_{\rm IGM})(Ar-1)}\right]$$
$$J_{g,g} = \frac{1}{T}\left[\frac{1 + (n-1)Ar}{Ar-1}\right]$$
$$J_{g,s} = 0$$
$$J_{s,Z} = -\frac{1}{T}\left[\frac{27}{50}\frac{rnE}{(Br + Z_{\rm IGM})(Ar-1)}\right]$$
$$J_{s,g} = -\frac{1}{T}\left[\frac{27}{50}\frac{nr}{Ar-1}\right]$$
$$J_{s,s} = -\frac{1}{T}.$$

Clearly, J has a singularity at $Ar - 1$ as expected from Equation (22) and it has an eigenvalue -1. The convergence to the equilibrium solution occurs on the timescale T if the other two eigenvalues have real components that are smaller or equal to this eigenvalue. The general expression for the eigenvalues of J is rather lengthy and we do not reproduce it here. Instead, we compute the real part of the eigenvalues numerically using the default parameters for A, B and $Z_{\rm IGM}$. The parameter B depends on ζ and thus on halo mass. We adopted $\zeta = 0$ which results in the most stringent limit on stability.

We show in Fig. A1 the result of our numerical analysis for $n = 1$ and $n = 2$. The maximum of the real part of the eigenvalues is less than zero (and hence the equilibrium is stable) for any $r < 1/A$ as long as E is sufficiently small ($E \lesssim 0.5 - 1$). Hence, as long as the $\rm H_2$ fraction is not extremely sensitive to changes in the metal fraction, the equilibrium is stable.

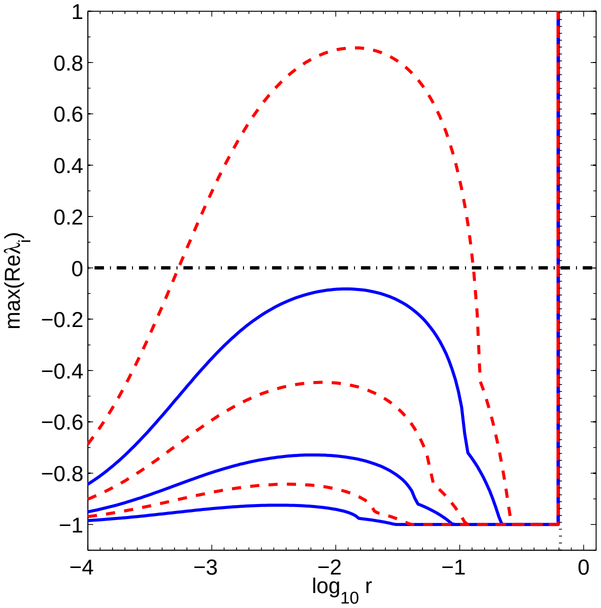

Figure A1. Maximum of the real part of the eigenvalues of JT as function of the ratio between SFR and gas accretion rate. The equilibrium is stable if the maximum of the real part of the eigenvalues is less than zero (horizontal dot-dashed line). Results for a linear ($n = 1$) star formation – $\rm H_2$ relation are shown by the three solid lines. The individual lines correspond to $E = 1$, $E = 0.3$, and $E = 0.1$ from top to bottom. Dashed lines show the corresponding results for a quadratic star formation – $\rm H_2$ relation. The equilibrium is stable for $r \lesssim 1/A$ (vertical dotted line) if $E \lesssim 0.5 - 1$ (depending on n), i.e., as long as the $\rm H_2$ fraction is not extremely sensitive to changes in the metal fraction.